Inorganic Chemistry

Article

pubs.acs.org/IC

Diarylethene-Containing Carbon-Rich Ruthenium Organometallics: Tuning of Electrochromism

Yifei Liu,[†] Cheikh Mbacké Ndiaye,[†] Corinne Lagrost,*[,†] Karine Costuas,*[,†] Sylvie Choua,[‡] Philippe Turek,[‡] Lucie Norel,[†] and Stéphane Rigaut*[,†]

[†]Institut des Sciences Chimiques de Rennes, UMR no. 6226 CNRS-Université de Rennes 1, Campus de Beaulieu, F-35042, Rennes, Cedex, France

[‡]Institut de Chimie, Université de Strasbourg, 1 Rue Blaise Pascal, BP 296 R8, F-67008 Strasbourg, Cedex, France

Supporting Information

ABSTRACT: The association of a dithienylethene (DTE) system with ruthenium carbon-rich systems allows reaching sophisticated and efficient light- and electro-triggered multifunctional switches R-[Ru]-C≡C-DTE-C≡C-[Ru]-R, featuring multicolor electrochromism and electrochemical cyclization at remarkably low voltage. The spin density on the DTE ligand and the energetic stabilization of the system upon oxidation could be manipulated to influence the closing event, owing to the noninnocent behavior of carbon-rich ligands in the redox processes. A combination of spectroscopic (UV−vis−NIR−IR and EPR) and electrochemical studies, with the help of quantum chemical calculations, demonstrates that one can control and get a deeper understanding of the electrochemical ring closure with a slight modification of ligands remote from the DTE unit. This electrochemical cyclization was established to occur in the second oxidized state (EEC mechanism), and the kinetic rate constant in solution was measured. Importantly, these complexes provide an unprecedented experimental means to directly probe the remarkable efficiency of electronic (spin) delocalization between two *trans* carbon-rich ligands through a metal atom, in full agreement with the theoretical predictions. In addition, when no cyclization occurs upon oxidation, we could achieve a redox-triggered magnetic switch.

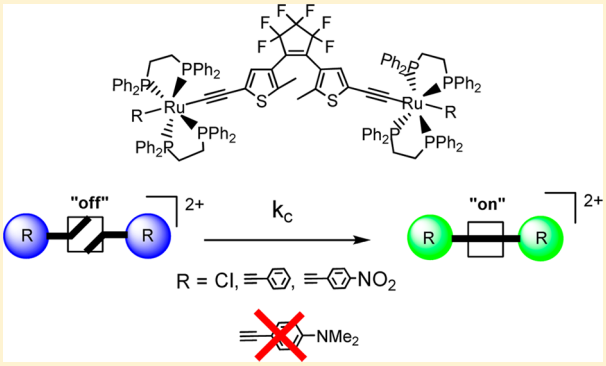

INTRODUCTION

Devices that can operate at the molecular level arose a great level of interest with the "bottom-up" approach expressed by Feynman in 1959.[1,2] In molecular-based switching devices, key physical properties can be modulated with external stimuli, such as light or electricity.[3] For instance, photochromic compounds that display a reversible transformation between two chemical forms with different properties present a high potential for application in switching devices.[3−8] In particular, among all photochromic units, the dithienylethene (DTE) system is an ideal system that presents a nonconjugated open form and a π-conjugated closed form, both thermally stable (Scheme 1).[4] Therefore, this system allowed the achievement of compounds with photogating of several properties[5,7] such as magnetic interactions,[9] molecular conductivity,[10,11] luminescence,[12] or other optical activities.[13] This DTE isomerization was also demonstrated to be effective on mechanical properties of crystals,[14] for organic electronic switching,[15] to achieve switchable organic nanoparticules,[16] logic gates,[17] or organogels.[18] Some DTE derivatives were also found to isomerize successfully in living organisms,[19] and one-color reversible control of the photochromic reactions was recently attained.[20]

In terms of increased functionality, particularly interesting is the control of molecule properties with several stimuli. In this context, the DTE unit is again attractive, as systems containing different types of these units can be potentially addressed selectively with different wavelengths, although it remains complicated to achieve.[21] Also, it has been shown that efficient electrochemical opening *or* closing can be reached with several systems,[22−28] depending on the relative stabilities of the open and closed forms of the electrochemically produced species (Scheme 1).

Scheme 1

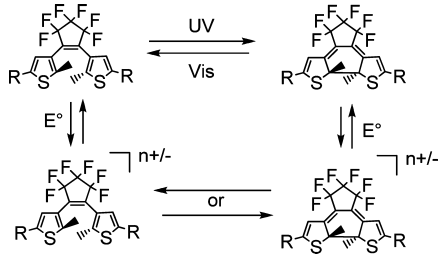

Received: June 4, 2014
Published: July 17, 2014

   dx.doi.org/10.1021/ic5013044 | *Inorg. Chem.* 2014, 53, 8172−8188

Scheme 2. Synthetic Pathways Yielding 1o−5o

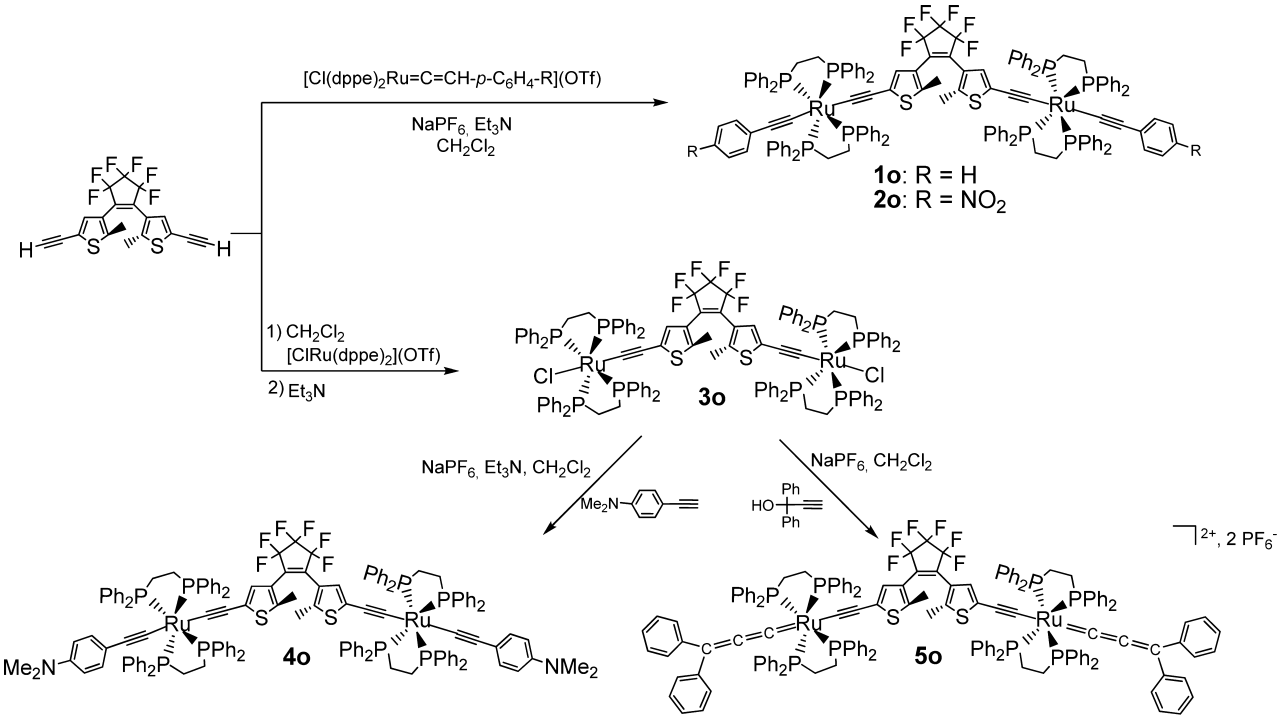

Original properties and high levels of functionalities may also be integrated into a molecular system through molecular engineering with the incorporation of one or several metal centers. This allows additional redox or photochemical addressing of the molecular component. Therefore, several associations of metal complexes with photochromic units have been carried out for the realization of molecular switches.[8,29−51] To this end, group 8 metal acetylide complexes, displaying strong ligand-mediated electronic effects, are attractive redox-switchable candidates.[52,53] Indeed, they allow modulation of different features such as NLO properties,[29,54] luminescence,[55] magnetic properties,[56] and conductivity[11] or achievement of quantum cell automata.[57] Among them, ruthenium species with a *trans* ditopic structure are especially attractive (i) owing to their exceptional ability to operate as a connector by allowing electron flow to occur between different elements in multi-component carbon-rich systems (i.e., provide a strong electronic interaction between two remote redox-active metal centers through a carbon-rich bridge or within a bridge),[52a,58−62] and (ii) for the achievement of efficient molecular wires and junctions.[11,63−66] In particular, using the fragment $[RuCl_2(dppe)_2]$ (dppe = 1,2-bis-(diphenylphosphino)ethane), we achieved polynuclear "W"-shaped molecular wires, up to 28 Å long, displaying a spin density uniformly distributed between the metal atoms and the carbon atoms of the chains in different oxidized/reduced states.[60,61] Therefore, with those metallic systems, the redox event that affects efficiently the entire carbon-rich architectures is expected to lead to the perturbation of any associated unit in a more efficient way than the ubiquitous ferrocenyl group.

In the search for such multiple controllable properties using these organometallics, we and others described associations between ruthenium/iron carbon-rich complexes and a DTE unit.[42−47] For example, in line and in parallel with our first observations,[43a] Akita and co-workers reported a light- and electro-triggered switch, [M]-DTE-[M] (M = CpRu(dppe)-C≡C-, CpRu(CO)(PPh_3)),[45,46] that displays an electrochemical cyclization occurring at significantly lower potential than that of organic systems owing to the strong electron delocalization upon oxidation in ruthenium species, an event not observed with the iron counterpart. Herein, we fully report our work on the synthesis and the study of bimetallic organometallic switches associating the DTE and the $[RuCl(dppe)_2]^+$ units (Scheme 2). Compounds **1o−5o** were designed in order (i) to gather efficient photochromism and multicolor electrochromism, both being attractive properties for optoelectronic devices, and (ii) to modulate the spin density on the DTE unit upon oxidation to control and also to get a deeper understanding of the electrochemical cyclization process. Therefore, using a combination of spectroscopic (UV−vis−NIR−IR and EPR), electrochemical, and theoretical techniques to study their different oxidation states, we illustrate the efficient photochromism and multicolor electrochromism of compounds **1o−4o** and the remarkable influence of the remote *trans* carbon-rich ligand on the efficiency of the electrochemical cyclization process. Hence, for the first time, we provide strong evidence that electrochemical cyclization occurs in the second oxidized state (EEC mechanism) along with a measure of the kinetic rate constants of the closing event in solution, whereas cyclization in the first oxidation state is the commonly accepted mechanism for organic units (ECE mechanism).[23] Significantly, the present study (i) shows that modification of a substituent remote from the DTE unit (∼16 Å) has a strong influence on the spin density distribution over the conjugated path through the ruthenium atom and on the energetic stabilization of the systems and (ii) reveals the experimental sensing of the spin density on the DTE unit with the determination of the closing kinetic rate constant, in agreement with the theoretical predictions. More generally, to the best of our knowledge, such a direct probing of spin density evidencing the remarkable efficiency of electronic delocalization between two *trans* carbon-rich ligands through a metal atom has never been reported

dx.doi.org/10.1021/ic5013044 | *Inorg. Chem.* 2014, 53, 8172−8188

Scheme 3. Synthetic Pathways Yielding 6

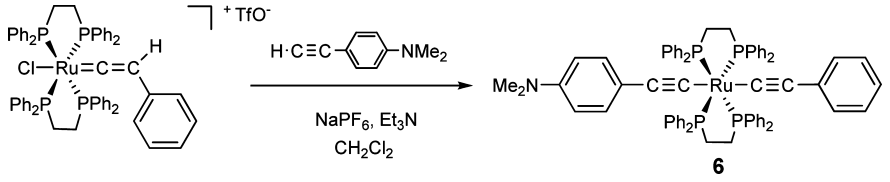

Scheme 4. Numbering Used for 1−4o/c^{n+}

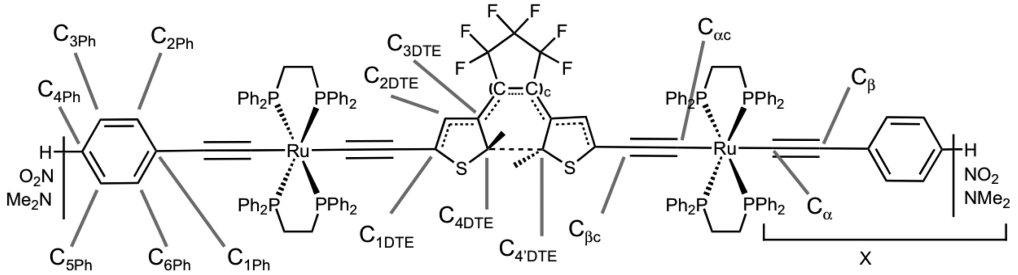

before. In addition, complex **4o**, in which oxidative electrocyclization is prevented, provides an unusual redox-triggered magnetic switch.

RESULTS AND DISCUSSION

1. Synthesis of Organometallic Switches. The synthetic routes to the targeted complexes **1o**−**5o** are displayed in Scheme 2. First, following the general procedure to prepare bis(σ-arylacetylide),[67] combinations of the diethynyl-substituted dithienylethene and the accurate vinylidene precursor in the presence of a noncoordinating salt ($NaPF_6$) and a base (Et_3N) led to the two bis(σ-arylacetylide) bimetallic complexes **1o** and **2o** (83% and 54% yield, respectively). Compound **3o** was achieved in 55% yield by activation of the same diethynyl-substituted dithienylethene with the 16-electron precursor [(dppe)$_2$RuCl](OTf), followed by addition of Et_3N to deprotonate the bis(vinylidene) intermediate. This latter complex **3o** was further reacted with Me_2N-*p*-C_6H_4-C≡CH, in the presence of $NaPF_6$ and Et_3N, to afford the bimetallic complex **4o** in 67% yield. Finally, the use of Ph_2(OH)C-C≡CH and $NaPF_6$ with **3o** led to the bis(acetylide-allenylidene) compound **5o** (50% yield). All these bimetallic species were characterized by means of ^{31}P, ^{1}H, and ^{13}C NMR, IR, and mass spectroscopies. FTIR measurement shows the expected characteristic $\nu_{(C\equiv C)}$ vibration stretch around 2040−2070 cm^{-1} for the acetylide functions with all compounds and additionally the allenylidene vibration stretch at 1924 cm^{-1} for **5o**. The *trans* arrangement on the ruthenium centers and their equivalence in each complexes were established by the observation of a single resonance peak in the ^{31}P NMR spectra for the eight phosphorus atoms in the typical regions for σ-arylacetylides (**3o**), bis(σ-arylacetylide)s (**1o**, **2o**, **4o**), bis-(acetylide-allenylidene)s (**5o**) at ca. δ = 50, 55, and 44 ppm, respectively. The ^{1}H NMR spectra also indicate that complexes are symmetrical, as expected: the ^{1}H NMR spectra of compounds **1o**−**5o** display for the photochromic bridge a single characteristic resonance for the methyl protons around δ = 1.7 ppm and one resonance for the two protons on the thiophene units around δ = 6.7 ppm. It is worth noting that dithienylethenes can adopt two conformations with the two thiophene rings in mirror symmetry (parallel conformation) or in C_2 symmetry (antiparallel conformation) and that the photocyclization reaction can proceed only from the antiparallel conformation.[4] Importantly, on the basis of ^{1}H and ^{31}P NMR characterizations, only one isomer is observed for steric reasons, the antiparallel one (*vide infra*).

2. Quantum Chemical Calculations. The geometric, electronic, and physical properties of complexes **1**−**4o**/**c**$^{0/2+}$ were studied by means of density functional calculations (DFT) to understand their electronic structures and physical behavior, in particular to elucidate the electrochemical isomerization process upon the second oxidation (*vide infra*). According to the results presented below, it is worth considering the complete series of the NMe_2-substituted systems **4o**/**c**$^{0/+/2+/4+}$. Also, for a better understanding of these oxidation processes of **4o**/**c**, the monometallic parent [($C_6H_4NMe_2$)-C≡C-(dppe)$_2$Ru-C≡C-(C_6H_5)] (**6**) was synthesized and investigated theoretically (Scheme 3). By studying **6**$^{0/+/2+}$, we aim to assess the role of the organometallic fragment connected to the NMe_2-bearing ligand.

Neutral Open Complexes. The study of the optimized geometries of **1o**, **2o**, and **4o** reveals that the structural arrangement of the central DTE moiety is very similar for these three systems. The main structural data are given as Supporting Information (Table S2). The dppe units were modified to lower the computational cost. Actually, this substitution of the phenyl end-group in the aryl-ethynyl series does not affect significantly the geometry of aryl-acetylide end-groups. This fact was previously observed in the related monometallic series [(R-C_6H_4)-C≡C-(dppe)$_2$Ru-Cl] (R = organic acceptor or donor groups).[68] The optimized chloro complex **3o** shows a slightly different geometrical arrangement of the DTE unit. The dihedral angles formed by the thiophene units and the central ethenyl bond are much larger (~90° for **3o** vs ~45° for **1o**, **2o**, and **4o**) and the C=C central bond is slightly shorter (1.354 Å vs 1.373−1.375 Å). Overall, the DTE unit in **3o** has a more pronounced single−double-bond alternation. Interestingly, for the whole series, the $C_{\alpha c}$≡$C_{\beta c}$ and $C_{\beta c}$−C_{1DTE} (see Scheme 4 for numbering) bond lengths are almost equal. Indeed, only the shorter Ru−$C_{\alpha c}$ distance reflects the effect of the Cl acceptor end-groups for **3o** compared to the substituted aryl-ethynyl end-groups (2.030 Å vs 2.093−2.100 Å).

The electronic structures of these compounds can be understood as the perturbation of the classical electronic

dx.doi.org/10.1021/ic5013044 | Inorg. Chem. 2014, 53, 8172−8188

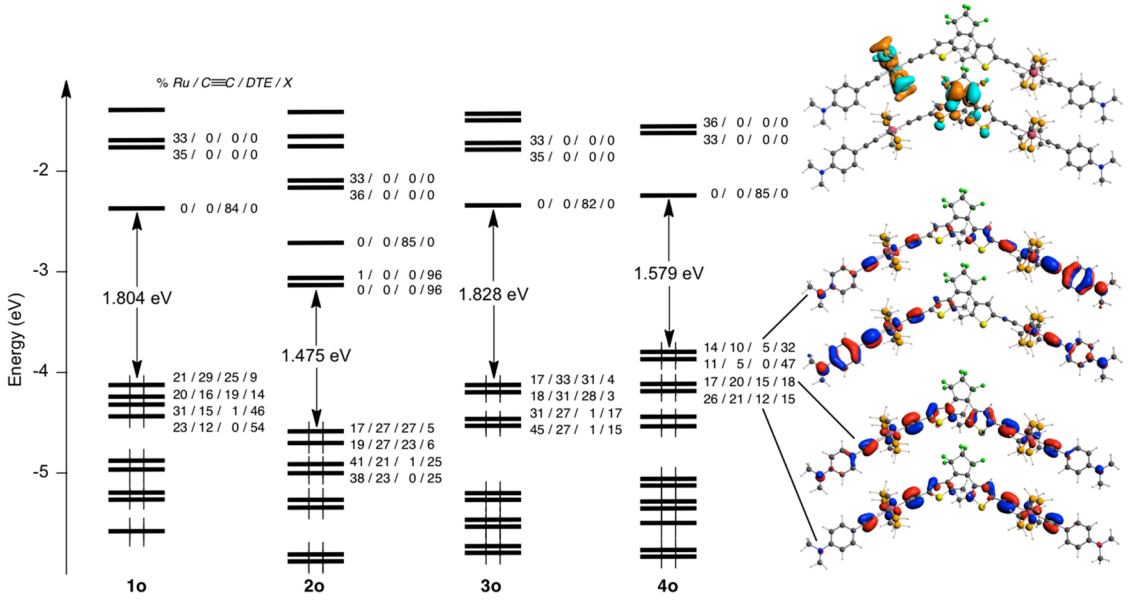

Figure 1. Molecular orbital diagrams of **1o**, **2o**, **3o**, and **4o**. Atomic Mulliken percentages: Ru = $\{Ru\}_2$; C≡C = $\{C_{ac} + C_{\beta c}\}_2$; DTE = $\{C_{1DTE} + C_{2DTE} + C_{3DTE} + C_{4DTE} + S\} + (C{=}C)_c$; X = Cl or $\{C_\alpha + C_\beta + C_2 + C_3 + C_4 + C_5 + C_6 + N + O$ or $C(Me)\}_2$ (see Scheme 4 for numbering). Contour plots of the orbitals from the HOMO−3 to the LUMO+1 of **4o** (0.03 $(e/bohr^3)^{1/2}$).

Table 1. Distances between C_{4DTE} and $C_{4'DTE}$ in Å and DFT Mulliken Atomic Spin-Densities Calculated for C_{4DTE} and $C_{4'DTE}$ Using the B3LYP Functional (See Scheme 4 for Labeling) for $1o^{2+}$, $2o^{2+}$, $3o^{2+}$, and $4o^{2+}$ in Electrons (e)

	$1o^{2+}$		$2o^{2+}$		$3o^{2+}$		$4o^{2+}$	
$d(C_{4DTE}{-}C_{4'DTE})$	3.687		3.720		3.745		3.655	
spin state	HS	BS	HS	BS	HS	BS	HS	BS
C_{4DTE}	+0.10	+0.10	+0.13	+0.13	+0.17	+0.17	+0.04	+0.04
$C_{4'DTE}$	+0.10	−0.10	+0.13	−0.13	+0.17	−0.18	+0.04	−0.04

Scheme 5. Photocyclization and Electrochemical Cyclization of 1o−4o

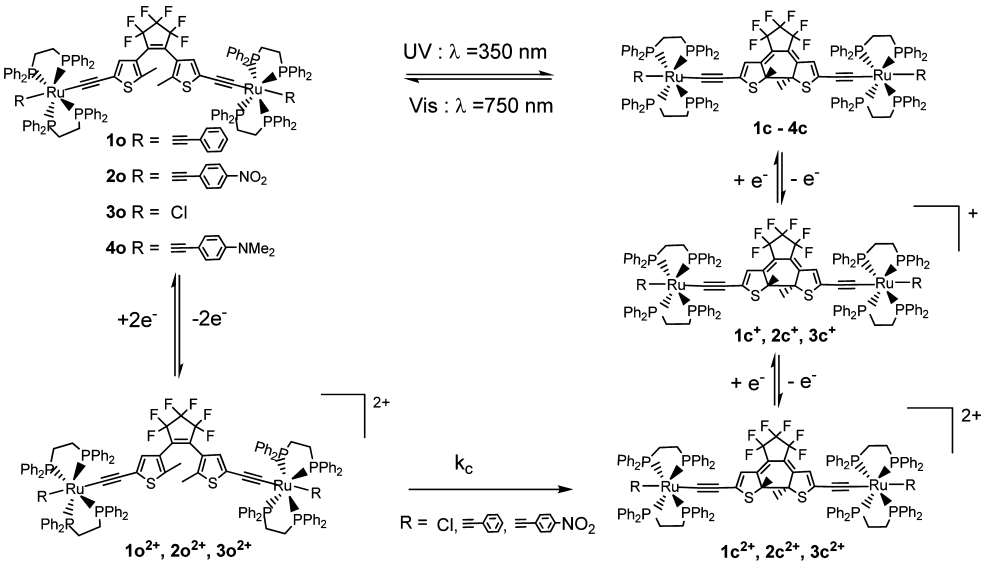

structure encountered in pseudo-octahedral $\{[XRu(dppe)_2]$-$(C{\equiv}C)\}$-containing systems by its coordination to a DTE unit.[68] Indeed, in all cases, the t_{2g} sets of occupied orbitals are found in the HOMO region and the e_g*, which are Ru−P antibonding, in the LUMO region. Also, as shown previously for similar systems, the increase of the donor character of the substituent X involves a global destabilization of the molecular orbitals and a larger participation of the X substituent up to almost 50% in the case of X = C≡C-$C_6H_4NMe_2$ (**4o**) (Figure 1). The DTE central unit participates in the t_{2g} orbitals, which have the appropriate symmetry to overlap with its π-system. The LUMO of those systems is the π* of the DTE, except for X = C≡C-$C_6H_4NO_2$, for which the two first unoccupied orbitals are NO_2 in character.

Dicationic Complexes. The dicationic open-DTE-containing complexes $\mathbf{1o}^{2+}$, $\mathbf{2o}^{2+}$, $\mathbf{3o}^{2+}$, and $\mathbf{4o}^{2+}$ were considered in all the

dx.doi.org/10.1021/ic5013044 | Inorg. Chem. 2014, 53, 8172−8188

Scheme 6. Photochromic Electroactivable Magnetic Switch

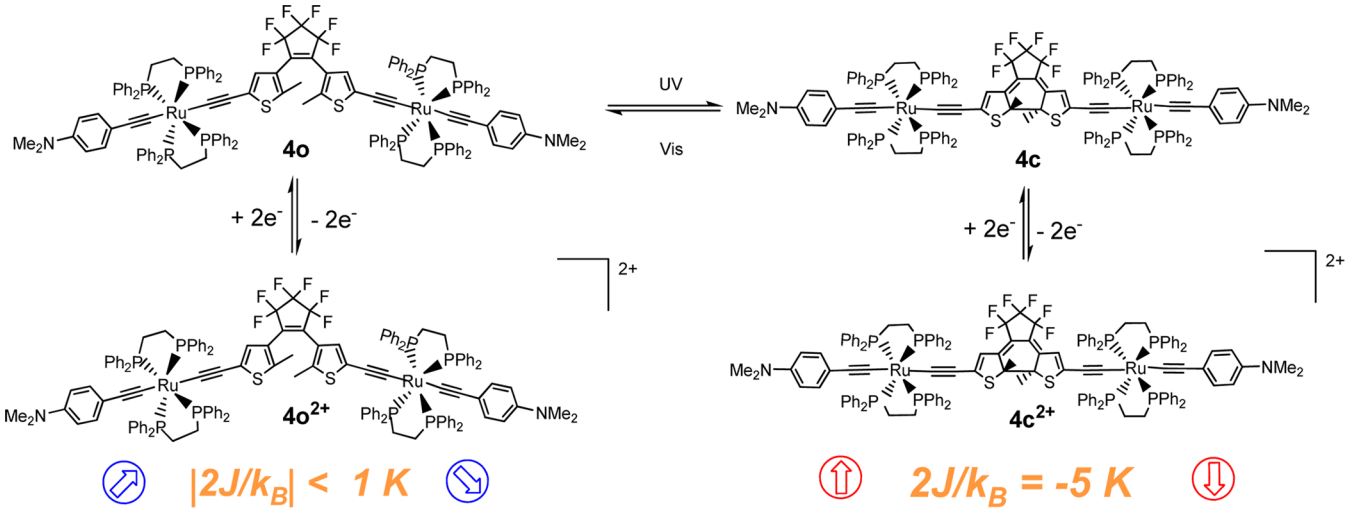

different spin states that they could adopt, i.e., closed-shell low-spin singlet state (LS), high-spin triplet state (HS), and open-shell singlet spin state (BS, two unpaired antiparallel electrons; see Experimental Part). Note that only the antiparallel arrangement of the organometallic branches toward the central C═C bond of the DTE was studied since we have shown previously that the parallel arrangement cannot exist because of the steric hindrance due to the phenyl groups of the dppe ligands.[43] The relative energies of the optimized open-DTE structures in their different spin states are reported in Table S3. In all cases, the diamagnetic LS state was found to be much higher in energy, regardless of the atomic basis set and functional used and will be not further considered. The energies of the HS and BS states are very close (<0.002 eV, 16 cm^{-1}). This allows considering that these systems are biradical compounds, i.e., possessing two spins hardly interacting.

When considering DTE isomerization, not only thermodynamics but also geometrical features have to be taken into account. The calculated distance separating the two reacting carbon atoms for each system is given in Table 1. It ranges between 3.655 and 3.745 Å, a length much less than the 4.2 Å limit above which cyclization cannot occur.[69] The electrochemical ring closure mechanism by an intramolecular radical coupling mechanism of complexes $\mathbf{1o}^{2+}$−$\mathbf{3o}^{2+}$ (see below, Scheme 7) is thermodynamically favorable by 0.064, 0.477, and 0.026 eV, respectively (energy ordering $\mathbf{2o}^{2+} \gg \mathbf{1o}^{2+} > \mathbf{3o}^{2+}$). This is not the case for the NMe_2-substituted system $\mathbf{4o}^{2+}$, which is 0.011 eV more stable than its closed form $\mathbf{4c}^{2+}$ (see Table 2), precluding cyclization from occurring electrochemically for **4o**. Of peculiar interest are the atomic spin densities of the two carbon atoms of the DTE unit that are forming a single C−C bond during the isomerization process (C_{4DTE}, $C_{4'DTE}$) via radical coupling. They are important in $\mathbf{1o}^{2+}$−$\mathbf{3o}^{2+}$ (ranging from 0.10 to 0.18 electron). On the contrary, the $C_{4'DTE}$ atomic spin density for the NMe_2-substituted system $\mathbf{4o}^{2+}$ is 0.05 electron (Table 1). Note that the quinoidal structure of the terminal phenyl group is more significant in $\mathbf{4o}^{2+}$ than for the rest of the series. On the basis of these values, the probability of having simultaneously the two unpaired electrons on C_{4DTE} and $C_{4'DTE}$ is decreasing in the order $\mathbf{3o}^{2+} > \mathbf{2o}^{2+} > \mathbf{1o}^{2+} \gg \mathbf{4o}^{2+}$. Associated with the energetic stabilization gained by the isomerization from $\mathbf{1o}^{2+}$−$\mathbf{3o}^{2+}$ to $\mathbf{1c}^{2+}$−$\mathbf{3c}^{2+}$ (energy ordering $\mathbf{2o}^{2+} \gg \mathbf{1o}^{2+} > \mathbf{3o}^{2+}$, see above), DFT results show that **2o** is

Scheme 7. Two Mechanistic Pathways for the Electrochemical Ring Closure

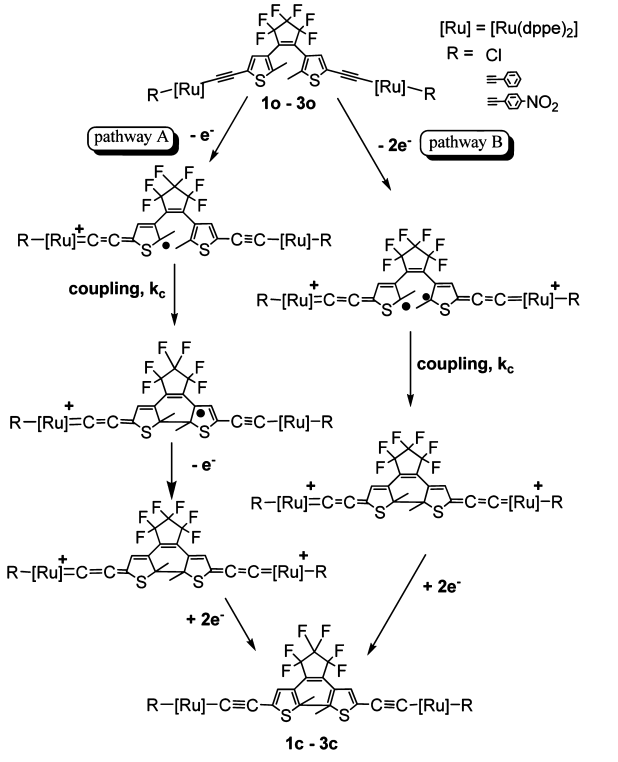

Table 2. B3LYP Relative Energy in eV of $\mathbf{4o}^{2+}$ and $\mathbf{4c}^{2+}$ in Their Different Spin States[a]

	spin state	E_{rel}
$\mathbf{4o}^{2+}$	LS	0.517
$\mathbf{4o}^{2+}$	HS	0.000
$\mathbf{4o}^{2+}$	BS	0.000
$\mathbf{4c}^{2+}$	LS	0.261
$\mathbf{4c}^{2+}$	HS	0.016
$\mathbf{4c}^{2+}$	BS	0.011

[a]LS = low spin; HS = high spin; BS = broken symmetry (see computational details).

dx.doi.org/10.1021/ic5013044 | Inorg. Chem. 2014, 53, 8172−8188

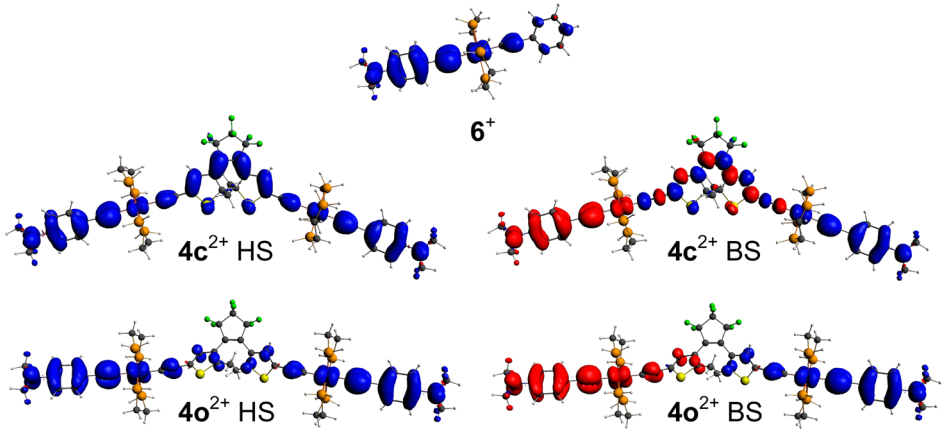

Figure 2. Contour plots of the spin density of **4c−o**$^{2+}$ in HS and BS spin states and **6**$^{+}$. Contour values: ±0.001 e/bohr^{3}.

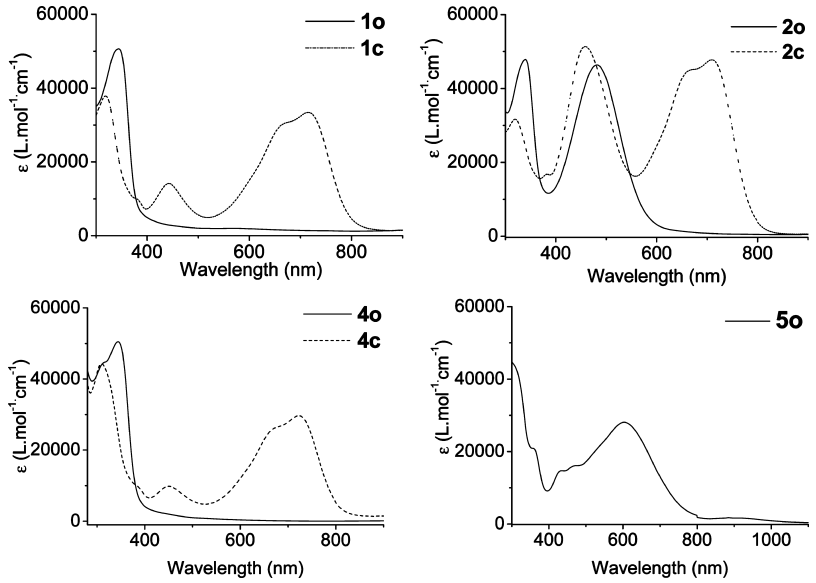

Figure 3. UV−vis absorption spectra of **1o**, **2o**, **4o**, and **5o** and spectral changes upon irradiation at λ = 350 nm (CH_2Cl_2). The initial spectrum was recovered after bleaching at λ = 750 nm ($[c] \approx 5 \times 10^{-5}$ mol L^{-1}).

the more readily electroisomerized, in full agreement with experimental results. The calculation of the activation barriers of the isomerization process for the dioxidized states would be necessary to discriminate which of **1o** and **3o** would isomerize more easily. Unfortunately, due to the size of the systems, this cannot be performed. Note that the activation barrier is supposed to be much higher in the neutral state than after oxidation.[6]

As stated before, **4**$^{2+}$, which possesses an electron-donating NMe_2 end-group, is more stable in its open form (see Table 2). The study of the spin states of **4**$^{2+}$ is thus particularly interesting to investigate computationally since both the open and the closed structure are electrochemically stable, auguring possible differences in the magnetic properties of both isomers (Scheme 6, see below). In principle, this necessitates a precise estimation of the singlet−triplet energy gap and thus performing a conformational study. Indeed, the $[(dppe)_2Ru]$ moieties, phenyl end-groups, and the thiophenyl of the DTE can easily rotate (along the single C−C bonds). Owing to the size of the system and the computational cost of an *ab initio* molecular dynamics study, this could not be envisioned. Nevertheless, general conclusions can be drawn by considering the order of magnitude of the energy differences. Indeed, **4o**$^{2+}$ has the same energy whatever the spin state, high spin or open-shell singlet (see Table 2). In that case, the magnetic properties should be those of a biradical compound with noninteracting spins. This can be nicely illustrated by the spin density plots given in Figure 2, which show a discontinuity in the spin density delocalization in the DTE unit. For **4c**$^{2+}$, the open-shell singlet is slightly more stable, by 0.005 eV (40 cm^{-1}), than the triplet state. In that case, an antiferromagnetic coupling is expected to be found experimentally. Interestingly, the plot of the spin density of **4c**$^{2+}$ BS shows that the unpaired electrons are mostly localized on the $RuC{\equiv}C\text{-}C_6H_4NMe_2$ branches (0.65 e) and coupled by a polarization mechanism (Table S4).

At this stage, a comparison with the monometallic analogous **6** is interesting. Indeed, the calculated mono-oxidized system presents a spin density localization of 0.80 e on its $Ru{-}C{\equiv}C\text{-}C_6H_4NMe_2$ part. More precisely, 0.42 e is found on the $Ru\text{-}C{\equiv}C$ chain (0.21 e on Ru), the rest being localized on the substituted phenyl group (0.13 e on NMe_2) (see Figure 2 and Table S4). This is clearly similar for the bimetallic **4o**$^{2+}$ compounds, for which the atomic ruthenium spin densities range between 0.18 and 0.20 e. Clearly, the oxidation affects

dx.doi.org/10.1021/ic5013044 | *Inorg. Chem.* 2014, 53, 8172−8188

Table 3. UV−Vis Data for Compounds 1−5 in CH_2Cl_2 ($[c] \approx 5 \times 10^{-5}$ mol L^{-1})

	UV−vis data, λ_{max}/nm (ε/L mol^{-1} cm^{-1})	closing/opening time (min)
1o	344 (50 200)	∼1/60
1c	318 (37 829), 442 (14 150), 688 (31 322) (sh), 716 (33 421)	
2o	340 (48 859), 482 (44 554)	∼1/300
2c	320 (31 675), 458 (51 338), 660 (44 524) (sh), 714 (47 553)	
3o	344 (28 280)	∼1/135
3c	315 (18 186), 432 (12 218), 688 (23 750) (sh), 718 (25 767)	
4o	316 (44 729), 344 (50 500)	∼1/60
4c	310 (44 391), 450 (9852), 686 (26 881) (sh), 722 (29 690)	
5o	311 (43 049), 363 (20 423), 605 (28 107)	no closing

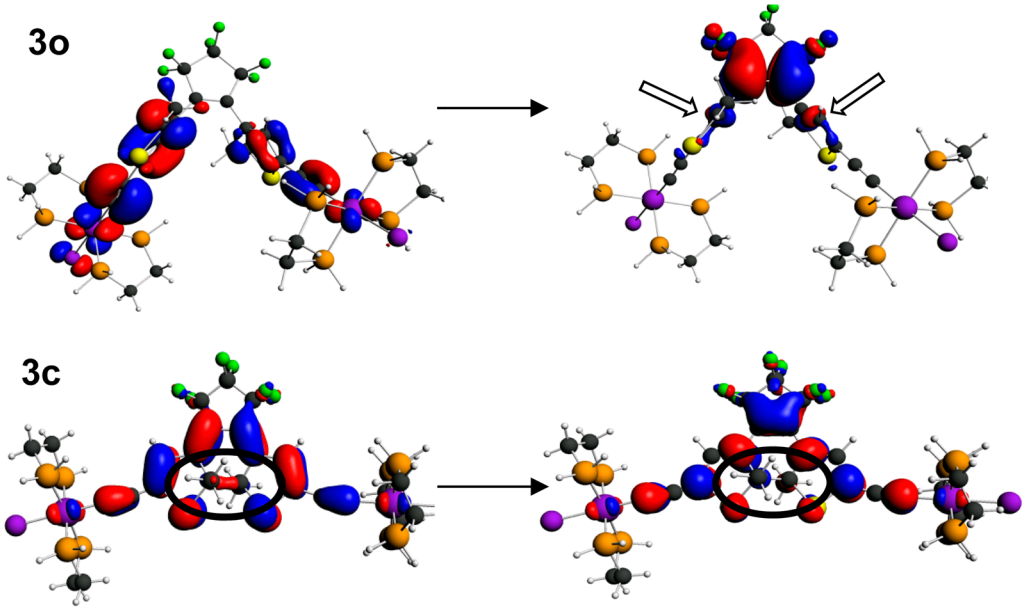

Figure 4. Main electronic transition contribution of the first excitation of **3o** (top) and **3c** (bottom). Contour values: ±0.03 $(e/bohr^3)^{1/2}$.

more strongly the substituents than for the rest of the series (**1**−**3o**$^{2+}$), diminishing subsequently the effect of oxidation on the Ru center. This makes possible a second one-electron reversible oxidation for **6** (as observed experimentally), which is not the case for other known monometallic [Ru(dppe)$_2$] systems. The spin density distribution for **6**$^{2+}$ in its HS state is 1.20 e on its Ru-C≡C-$C_6H_4NMe_2$ part and 0.29 e on Ru, the rest being on the other *trans*-acetylide branch. One can consider that **6** can be oxidized twice, the whole Ru-C≡C-$C_6H_4NMe_2$ being the redox moiety. For **4o**$^{4+}$, the average atomic ruthenium spin density is 0.31 e, which is a value really close to that found for **6**$^{2+}$. The rest of the atomic spin densities on the Ru-C≡C-$C_6H_4NMe_2$ parts are indeed really similar between **4o**$^{4+}$ and **6**$^{2+}$ (see Table S4).

Oxidations of **4c** were also considered. Interestingly, the vacuum ionization potential of **4c** is only 4.362 eV, while it is calculated to be 5.196 eV for **4o**. Compound **4c**$^+$ is thus more stable than **4o**$^+$ by 0.359 eV, while the open system is the most stable arrangement of **4**$^{2+}$ but by only 0.011 eV. For the tetracations, **4c**$^{4+}$ (BS) is 0.342 eV more stable than **4o**$^{4+}$, also open-shell (HS and BS isoenergetic).

3. UV−Visible Spectra/Photoisomerization Studies. The five bimetallic adducts **1o**−**5o** display in CH_2Cl_2 and in toluene an intense absorption band with a large extinction coefficient at ca. λ_{max} = 345 nm (Figure 3, Table 3, Figure S7, and Table S1). Isomerization studies (Scheme 5) were conducted in CH_2Cl_2 (Figure 3, Figure S7, Table 3) and toluene (Table S1). This process, complete and reversible with **1o**−**4o**, leads to the very stable **1c**−**4c** complexes in the UV−vis cell ($[c] \approx 5 \times 10^{-5}$ mol L^{-1}). Typically, upon irradiation of **1o** with UV light (350 nm) in the band related to transitions implicating the DTE unit at ca. 340 nm, this band vanishes while a broad absorption assigned to the deep green closed isomer **1c** appears at λ_{max} = 710−720 nm with a shoulder at 680−690 nm. These solutions of the closed forms can be further bleached to the open-form solutions under visible light (750 nm), with quantitative recovering of the initial spectra.

The theoretical studies previously reported for **3o** have revealed that its first excited state mainly corresponds to a HOMO ($Ru_{d/\pi}$) → LUMO (DTE_{π^*}) allowed excitation (see Figure 4).[43,70] This d/π(RuC≡C) to π^*(DTE) excitation induces enough accumulation of density on two carbon atoms of the DTE for the creation of a single C−C bond upon rotation. The band located at λ_{max} = 462 and 312 nm for **2o** and **4o**, respectively, are related to charge transfers from the ruthenium to the ligand bearing the nitrobenzene or *N*,*N*-dimethylaniline groups.[68] For **3c**, the first excited state could also be described by TD-DFT calculations.[43] It is mainly described by a HOMO to LUMO transition. As shown in Figure 4, this $M_{d/\pi}$-C_2DTE_{π} → $M_{d/\pi}$-$C_2DTE_{\pi^*}$ transition induces loss of bonding density between the methylated carbon atoms and thus eventually bond breaking. The conformational study performed on **3c** has also revealed that several rotamers of close energy are found for its ground state (Ru(dppe)$_2$

dx.doi.org/10.1021/ic5013044 | Inorg. Chem. 2014, 53, 8172−8188

rotations toward the DTE plane). This explains the unusual broadening of the lower lying band of the experimental spectrum. Indeed, for some rotamers, the first excited state is found as an admixture of $M_{d/\pi}$-C_2DTE_{π} → M_d-$dppe_{\pi^*}$ and $M_{d/\pi}$-C_2DTE_{π} → $M_{d/\pi}$-$C_2DTE_{\pi^*}$ transitions. The broad experimental band at 680−720 nm observed for the closed systems can thus be described as the envelope of the spectra of the different isomers present in solution.

Complete conversions were also observed with the help of ^{31}P and ^{1}H NMR studies in C_6D_6 ($[c] \approx 2 \times 10^{-3}$ mol L^{-1}), namely, with the characteristic upfield and downfield shifts of the thiophene and methyl group protons, respectively, and a slight upfield shift of the phosphorus atom resonance (Table 4, Figure S8). The $\nu_{(C\equiv C)}$ vibration stretch is also systematically shifted upon ring closure to a lower wavenumber by 20−40 cm^{-1}, which is consistent with an increased conjugation.

Table 4. ^{1}H and ^{31}P NMR Chemical Shift Data for Compounds 1−4 (C_6D_6)

	^{1}H NMR		^{31}P NMR	IR
	δ CH^{DTE} (ppm)	δ CH_3^{DTE} (ppm)	dppe (ppm)	$\nu_{(C\equiv C)}$ (cm^{-1})
1o	6.74	1.99	55.0	2035
1c	5.67	2.64	54.3	2012
2o	6.75	1.99	54.4	2043
2c	5.79	2.63	53.8	2019
3o	6.55	1.95	50.7	2055
3c	5.43	2.61	49.5	2009
4o	6.73	2.00	55.1	2051
4c	5.66	2.66	54.4	2009

For the cumullenic compound **5o**, the additional broad transition in the visible region (λ_{max} = 605 nm) is expected to arise from the allowed transition from one of the partially metal based HOMOs to an unoccupied orbital mainly delocalized over the allenylidene ligand(s), thus with $Ru^{II}(d\pi)$→ π^*-(allenylidene) MLCT character.[71] However, the isomerization study shows that complex **5o** does not lead to photocyclization.[72] This is most probably because of internal conversion processes of de-excitation to the lower lying excited states, known to be much faster than atomic motion, that do not involve the DTE unit but rather the allenylidene functions (*vide supra*).

It has to be noted that for other types of ruthenium-containing DTE systems, De Cola and collaborators have proposed two competitive photocyclization paths, one occurring via a triplet intraligand (^{3}IL) excited state and a second one via the singlet ^{1}IL excited state. This was later proved by time-resolved-spectroscopy experiments for Ru(bpy)$_3$ derivatives and proposed theoretically for Akita's systems (depending on the ordering of the excited states).[73] Nevertheless, these double mechanisms cannot be generalized to all transition-metal-containing compounds since it depends on (i) the ordering and the nature of the excited states and (ii) the spin−orbit coupling strength between ^{1}MLCT and ^{3}MLCT excited states.[74] In the particular case of the systems **1**−**4**, the first excited state can be described as a d/π(RuC≡C) to π^*(DTE) (mixed IL and MLCT) state that shows sufficient accumulation of electronic density to induce ring closure.

4. Electrochemical Studies. Cyclic voltammograms (CV) were recorded for compounds **1o**−**5o**. While compounds **1o**, **2o**, and **3o** display closely related behaviors, **4o** and **5o** exhibit significantly different behaviors in their redox properties. As illustrated in Figure 5a for compound **1o**, at low and moderate

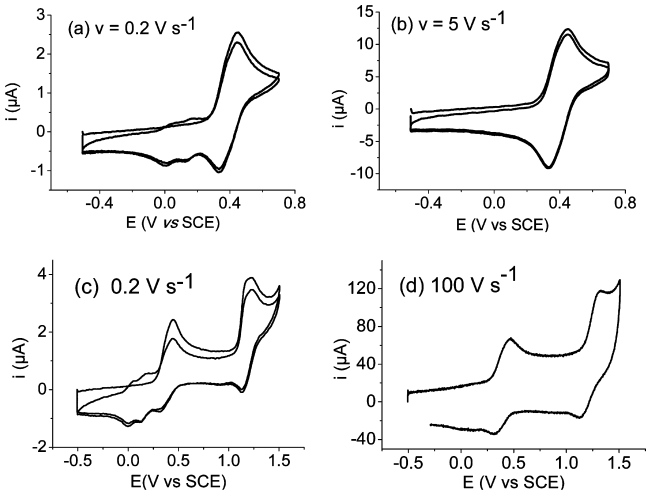

Figure 5. Two consecutive CV traces of **1o** in CH_2Cl_2 (7.10^{-4} mol L^{-1}, 0.2 mol L^{-1} Bu_4NPF_6) at a Pt electrode at different scan rates: (a and c) ν = 0.2 V s^{-1}, (b) ν = 5 V s^{-1}, and (d) ν = 100 V s^{-1}.

scan rates (0.1−2 V s^{-1}), the voltammograms of **1o**, **2o**, and **3o** show a broad and partially reversible wave located at ca. 0.4−0.55 V, which is typical of ruthenium acetylide oxidation.[66−68] The CV shape suggests that it is composed of two slightly separated one-electron oxidations for the two electronically independent metal fragments with ΔE° = 75−85 mV (*vide infra*). Consecutively, two new redox systems appear at less positive potentials on the return scan. These new redox systems are well separated and correspond to two reversible processes, as can be seen on the following scan. Upon increasing the scan rates, these two new redox systems do not appear, while the broad oxidation wave becomes fully reversible (Figure5b), the full reversibility being observed at 2, 50, and 30 V s^{-1} for **1o**, **2o**, and **3o**, respectively. These observations suggest that the closed forms of compounds **1**, **2**, and **3** are electrochemically generated from the oxidation of the open isomers on the time scale of the cyclic voltammetry and that cyclization occurs at different kinetics for each compound. Differences between the standard potentials for the two primary oxidation processes (broad wave), $\Delta E = E_{o1}^\circ - E_{o2}^\circ$, were extracted from the partially and fully reversible voltammograms with the use of a working curve[75] and of numerical simulations of the voltammograms.[76] The values of the standard potentials, E_{o1}° and E_{o2}°, for the open compounds were subsequently derived, while the corresponding values for the closed compounds (E_{c1}° and E_{c2}°) were straightforwardly determined from the low scan rate CVs (Table 6). Note that compound **2o** presents more positive oxidation potential values due to the electron-withdrawing effect exerted by the nitro group.

It is also worth noting that an additional broad anodic peak is observed for potential values more positive than 1 V (Figure 5c and Table 6), due to the signatures of both open and closed forms. This potential value is strongly reminiscent of the usual oxidation potential reported for the DTE core,[22−25] and the larger potential window at this scan rate allows larger partial ring closing on the return scan than that observed in Figure 5a. At a high scan rate, this second peak is no longer broad and, therefore, characteristic of the open form (Figure 5d). This allows the assignation of the peak to the open forms (E_{o3}°) and

dx.doi.org/10.1021/ic5013044 | Inorg. Chem. 2014, 53, 8172−8188

Table 6. Electrochemical Data for Compounds 1−5[a]

	$E_{or}°$ (V)	$E_{o1}°$ (V)	$E_{o2}°$ (V)	$\Delta E°$ (mV)	$E_{o3}°$ (V)	$E_{cr}°$ (V)	$E_{c1}°$ (V)	$E_{c2}°$ (V)	$\Delta E°$ (mV)	$E_{c3}°$ (V)	$E_{c4}°$ (V)	k_c (s^{-1})
1		0.356	0.430	75	1.230		0.020	0.150	110	1.195		0.5
2		0.495	0.575	80	1.490[b]		0.135	0.230	95	1.360		25
3		0.405	0.490	85	1.505[b]		0.009	0.130	119	1.480		15
4		0.145[c]	0.600[c]	36[d]	1.340[b]		−0.007	0.113	200	0.569	1.040	0
5	−0.510				1.078[c]	−0.510	0.575	0.640	65			
6		0.121	0.598									

[a]V vs SCE. Conditions: CH_2Cl_2 + 0.2 M NBu_4PF_6, 20 °C, Pt electrode. Decamethylferrocene was used as an internal probe with $E°$ = −0.140 V vs SCE. [b]Anodic peak potential for an irreversible process for v > 200 V s^{-1}. [c]Two-electron process. [d]Statistical peak potential separation of the two one-electron processes composing the $E_{o1}°$ and $E_{o2}°$ waves.

of the shoulder at lower potential observed at lower scan rate to the corresponding closed form ($E_{c3}°$).

To confirm the closing event, controlled-potential macroelectrolyses were further performed on the open compounds at 0.6 V for **1o** and **3o** and at 0.7 V for **2o**. After a two-electron oxidation, the broad system vanishes and only the two new redox systems at less positive potentials are observed along with the shift of the higher potential wave, as observed in CV experiments (Figure S9). The dicationic forms were not isolated as they are not stable enough. Further two-electron reduction of the anolyte and workup of the solution followed by ^{31}P NMR and UV absorption measurements confirmed the conversion of the open compounds into their closed forms, showing the efficiency of the electrochemical cyclization process. Note that clean mono-oxidation of the complexes is not possible owing to the small separation (80 mv) of the two redox events. This would lead to a mixture of the three possible redox forms, and closing of the dicationic form would shift the equilibrium to a 50/50 open neutral/closed doubly-oxidized mixture. UV irradiation at λ_{max} = 350 nm of the open isomers was also performed in the electrochemical cell. Comparison of the different cyclic voltammograms (Figure 6) also validates the

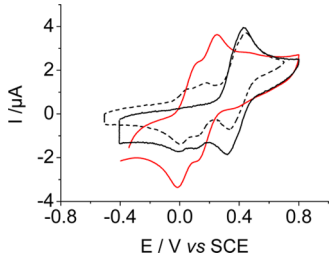

Figure 6. CV of **1o** ([C] = 10^{-3} mol L^{-1}, 0.2 mol L^{-1} Bu_4NPF_6, v = 0.2 V s^{-1}) at a Pt electrode (black solid line), after a 50 s microelectrolysis at 0.55 V (dotted line) and after UV irradiation at λ_{max} = 350 nm (red line).

fact that the two reversible well-separated redox systems correspond to the oxidation/reduction waves of the closed form, **1c** to $\mathbf{1c}^+$ and $\mathbf{1c}^+$ to $\mathbf{1c}^{2+}$ (same for **2c** and **3c**). The fact that the electrochemical processes of the closed compounds occur at less positive potentials than those of the open form falls in line with the more extended π-conjugated structure of the closed forms relative to the open ones and with the quantum chemical results. The wave separation of the two redox events ($\Delta E° = E_2 - E_1 = (-RT/F) \log Kc$) is a thermodynamic parameter describing the increased stability of the intermediate state with respect to disproportionation, allowing the observation of this first oxidized state (*vide infra*). In addition, if compounds **1o−3o** are submitted to a preelectrolysis at their first oxidation states for 10 s, further fast CVs recorded between −0.7 and 0.3 V do not exhibit the redox waves corresponding to the ring-closed isomer. On the contrary, if pre-electrolysis takes place at the potential of the second oxidation state, the signal of the ring-closed isomer is then observed (Figure 7). This observation qualitatively indicates that ring closure should rather occur in the second oxidized states $\mathbf{1o}^{2+}$−$\mathbf{3o}^{2+}$ (*vide infra*).

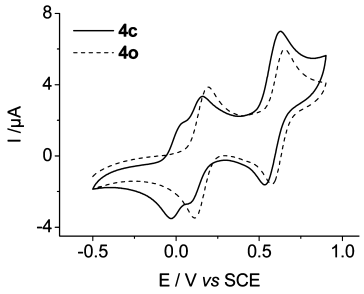

Figure 7. CV of **4o** and **4c** after UV irradiation at λ_{max} = 350 nm ([c] = 7.10^{-4} mol L^{-1}) in CH_2Cl_2 (0.2 mol L^{-1} Bu_4NPF_6, v = 0.2 V s^{-1}) at a Pt electrode.

The electrochemical study of compound **4o** shows very different CVs, as compared to those of compound **1o−3o**, as it does not lead to the electrochemical-driven ring-closing reaction (Figure 7). Over the scan rate range 0.2−900 V s^{-1}, two separate reversible, two-electron oxidation processes are observed at 0.145 and 0.600 V ($\Delta E_p \approx$ 60−65 mV).[77] In order to better understand those oxidation processes, [$(C_6H_4NMe_2)$-C≡C-$(dppe)_2$Ru-C≡C-(C_6H_5)], (**6**) was also studied. It exhibits two separate one-electron, reversible oxidation waves located at 0.13 and 0.60 V, similarly to **4o** (Figure S10). These two waves correspond to two one-electron oxidations of the whole Ru-C≡C-$C_6H_4NMe_2$ redox moiety (*vide supra*). Thus, because the open isomer **4o** is a nonconjugated molecule, the two carbon-rich arm systems at each side of the molecule behave as two identical and independent moieties that are concomitantly oxidized during the two processes. The peak potential separation for both processes is then probably $\Delta E° = E°_1 - E°_2$ = 35.6 mV.[78] UV irradiation at λ_{max} = 350 nm of **4o** performed in the electrochemical cell allowed the observation of the electrochemical properties of **4c** (Figure 7). While the second two-electron oxidation wave remains unaffected, the first one is split in two one-electron oxidation waves at lower potential, which is consistent with the double oxidation now involving a conjugated (central) pathway. Because the second wave remains unaffected, this process probably involves mainly the Ru-C≡C-$C_6H_4NMe_2$ moieties, as revealed by DFT calculations. Complex **4o** also displays a third, almost

dx.doi.org/10.1021/ic5013044 | Inorg. Chem. 2014, 53, 8172−8188

irreversible oxidation wave at E_{pa} = 1.34 V, which probably yields partial ring closure, as a reduction wave (E_{pc} = 1.015 V) corresponding to the reversible fifth oxidation of the closed form **4c** ($E°$ = 1.040 V) is observed on the return scan (Figure S11). Unfortunately, the instability of the resulting highly charged species did not allow further quantitative investigations.

Finally, the cumullenic compound **5o** displays an irreversible oxidation process at 1.078 V and the appearance on the return scans of two new slightly separated redox systems at less positive potentials (ca. 0.6 V, Figure 8). After a 60 s microelectrolysis at 1.1 V (inset of Figure 8), these two monoelectronic signals appear to be slightly separated reversible redox systems, with a separation of 65 mV (Table 6).[75] By comparison with **1o**−**3o**, these redox waves are believed to correspond to the two reversible one-electron oxidations of the electrogenerated closed form **5c**. In addition, a reversible two-electron-reduction process is observed at $E°$ = −0.510 V, suggesting that the two remote cumullenic parts are simultaneously reduced.[79] Note that over the scan rate range studied (0.1−500 V s^{-1}) the oxidative process remains totally chemically irreversible, suggesting that the ring-closing isomerization of **5o** is a fast reaction. Further investigation was made by performing a controlled-potential macroelectrolysis at 1.2 V. Surprisingly it was not possible to obtain the full conversion of **5o** into **5c** as for compounds **1o**−**3o**. A ∼50/50 mixture of open and closed forms was always obtained, suggesting that the relative stabilities of the intermediate in the closed and open forms are equivalent. As full electrochemical conversion to **5c** is not possible along with the fact that neither **5o** nor the electrogenerated **5c** was subject to photoisomerization, we did not carry out further studies on **5o**/**c**.

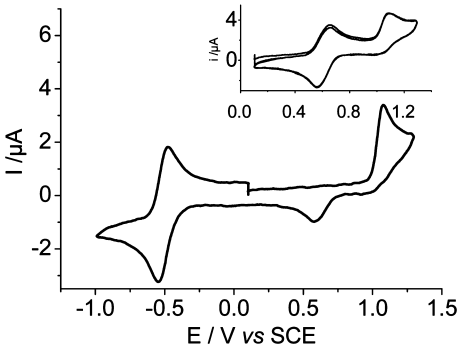

Figure 8. CV of **5o** ([c] = 10^{-3} mol L^{-1}) in CH_2Cl_2 (0.2 mol L^{-1} Bu_4NPF_6, v = 0.2 V s^{-1}) at a Pt electrode. Inset: after a 60 s microelectrolysis at 1.1 V.

5. Spectroelectrochemical Studies. The optical properties of **1o**−**4o** upon oxidation were investigated by UV/vis/NIR spectroscopies in an optically transparent thin-layer electrochemical (OTTLE) cell in CH_2Cl_2. For compounds **1o**−**3o**, the measurements show similar results (Table 7). As an example, upon two-electron oxidation of **1o** (Figure 9a, see Figures S13−S17 for other complexes), the intense absorption band at λ_{max} = 344 nm vanishes and two new bands attributed to the closed isomer $\mathbf{1c}^{2+}$ concomitantly show up with a main band at λ_{max} = 800 nm. Further electrochemical reduction leads to the clean spectrum of **1c** (λ_{max} = 718 nm). The reduction proceeds via $\mathbf{1c}^{+}$, which displays a remarkably broad absorption band in the NIR region from 750 to 1800 nm with λ_{max} = 1350 nm. On the basis of the TD-DFT calculations performed for **3**, these absorption bands are not attributed to intervalence charge transfer (IVCT), but rather to $\pi \rightarrow \pi^*$ transitions of the ligands with significant metal characters of the type HOMO−n → SOMO.[70] Note that two-electron oxidation of the **1c** solution to $\mathbf{1c}^{2+}$ leads to a spectrum identical (including intensity) to that obtained upon the first two-electron oxidation of **1o**, supporting the initial fast ring closure on the experimental time scale and attesting to the reversibility of the redox processes after closure. Therefore, these four redox states show very different absorption spectra, all obtained at low voltage (Table 7).

As **4o** does not lead to the electrochemical cyclization reaction, it is twice oxidized to the pale yellow stable state $\mathbf{4o}^{2+}$ when the oxidation potential is set to that of the first wave (Figure 7b, Table 6). The characteristic absorption band for **4o** at λ_{max} = 344 nm disappears, and two intense absorption bands appear at λ_{max} = 418 nm and λ_{max} = 1150 nm, whose nature remained uncertain until now. Further oxidation to $\mathbf{4o}^{4+}$ leads to an orange solution. The strong absorption band at the NIR region decreases and is blue-shifted (λ_{max} = 1040 nm). A new band at λ_{max} = 544 nm increases, while the band at λ_{max} = 418

Table 7. UV−Vis Data for Compounds 1o−3o, $\mathbf{1c}-\mathbf{3c}^{n+}$, $\mathbf{4o}^{2n+}$, and $\mathbf{6}^{n+}$ (n = 0, 1, 2) Obtained upon Spectroelectrochemical Analysis (0.2 mol L^{-1} Bu_4NPF_6 in CH_2Cl_2)

	λ_{max}/nm (ε/L mol^{-1} cm^{-1})					
	1	**2**	**3**		$\mathbf{4o}^{2n+}$	$\mathbf{6}^{n+}$
o	344 (50 200)	338 (46 001)	342 (28 856)	n = 0	344 (50 636)	326 (24 691)
		484 (48 294)				
$\mathbf{c}^{2+}$	414 (9487)	392 (46 283)	452 (13 227)	n = 1	418 (35 039)	420 (14 620)
	514 (12 217)	502 (28 867)	652 (20 192)		970 (12 736) (sh)	968 (8425) (sh)
	800 (21 969)	748 (39 429)			1150 (29 969)	1132 (17 358)
	1200 (3153)	1168 (3699)				
c	320 (32 542)	320 (43 826)	316 (13 022)	n = 2	544 (15 552)	562 (5295)
	444 (7822)	460 (61 734)	432 (8322)		930 (10 724)	932 (4792)
	688 (23 356)	660 (54 390)	688 (20 174)		1040 (14 997)	1164 (3504)
	718 (25 276)	710 (57 504)	720 (22 458)			
$\mathbf{c}^{+}$	568 (7002)	384 (30 592)	508 (8026)			
	1136 (21 859)	1144 (26 092)	994 (12 524)			
	1350 (26 686)	1352 (29 669)	1100 (12 961)			
			1350 (11 470)			

dx.doi.org/10.1021/ic5013044 | Inorg. Chem. 2014, 53, 8172−8188

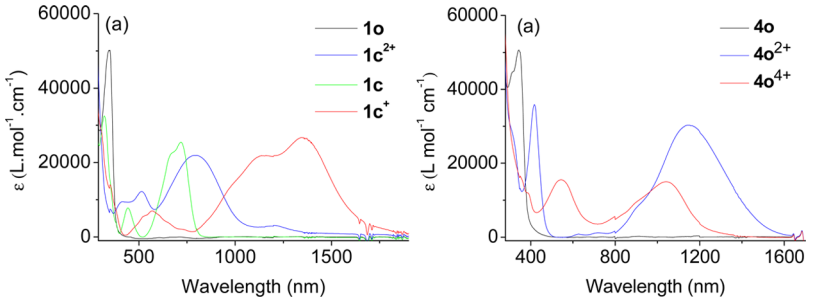

Figure 9. UV−vis−NIR absorption spectra obtained upon oxidation in an OTTLE cell with **1o** and **4o** (0.2 mol L^{-1} Bu_4NPF_6 in CH_2Cl_2).

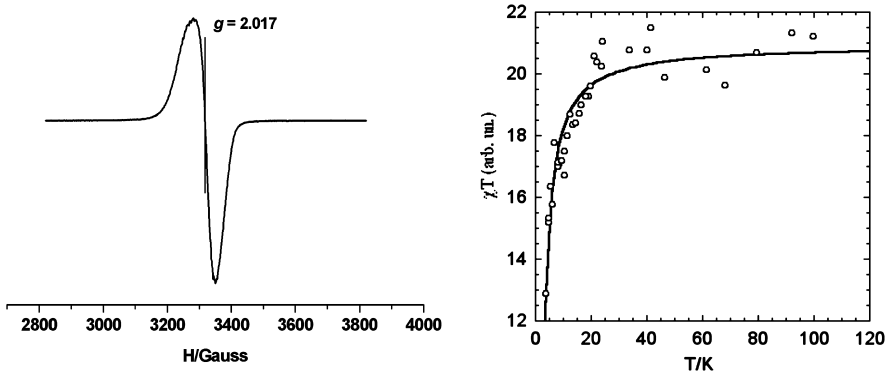

Figure 10. (a) X-band EPR spectrum of $\mathbf{4c}^{2+}$ in a frozen solution at 4 K in CH_2Cl_2 and (b) temperature dependence of the χT product (integrated EPR absorption).

nm disappears. On the basis of the absorption intensities, the reversibility is 100% for the first event and ca. 90% for the second. The experiment conducted with **6** is almost identical (Table 7, Figure S17), with the notable exception that the extinction coefficients are about half of those obtained with **4o**. These observations support the fact that the two ruthenium−carbon-rich arms of compound **4o** behave independently and that the properties are mainly driven by the whole RuC≡C-$C_6H_4NMe_2$ redox moieties.

Overall, these molecular DTE switches show a remarkably low potential electrochromism, especially significant in the NIR region owing to the delocalized nature of frontier orbitals between the ruthenium atoms and within the carbon-rich ligands, where several HOMO−n (n > 1) to SOMO transitions with a large $\pi \rightarrow \pi^*$ character take place.

6. Magnetic Properties. Since complex **4o** undergoes photocyclization but no electrochemical cyclization during the first two redox events, it is stable under four redox states: **4o**, $\mathbf{4o}^{2+}$, **4c**, and $\mathbf{4c}^{2+}$. Therefore, in contrast to **1o**−**3o**, it may be considered as a potential photomagnetic switch upon two-electron-oxidation stimulation (Scheme 6).[80] In order to measure the magnetic performance of this system, the chemical two-electron oxidations of **4o** and **4c** were carried out with two equivalents of $[Cp_2Fe][PF_6]$ in degassed CH_2Cl_2 at room temperature. Due to the limited solubility of $\mathbf{4o}^{2+}$, only a weak EPR signal centered around $g \approx 2.0$ is observed at low temperature, whereas $\mathbf{4c}^{2+}$ leads to an intense EPR spectrum with an asymmetric single line centered at g = 2.017 (Figure 10a and Figure S18). The isotropic nature of the signal observed for the two compounds is expected for such ruthenium carbon-rich complexes[60,68,81] and arises from the delocalization of the unpaired electron along the chain. Magnetic properties were investigated upon recording the temperature dependence of the integrated intensity of the EPR signal observed at around $g \approx 2$. The χT product (χ is the EPR susceptibility) of the closed form $\mathbf{4c}^{2+}$ shows a decrease when the temperature is lowered (Figure 10b). It is indicative of antiferromagnetic coupling between the two S = 1/2 spin carriers and can be well reproduced by a Bleaney−Bowers law for a singlet−triplet equilibrium, $\chi T = 3C/(3 + \exp(-\Delta E_{ST}/kT))$, with ΔE_{ST} the singlet−triplet gap and C and k the Curie and Boltzmann constants. The fitting yields a value of $\Delta E_{ST}/k$ = −5 K (3.5 cm^{-1}), which indicates a singlet ground state. The magnetic exchange pathway is obviously of intramolecular origin as previously discussed in related compounds with organic nitronyl nitroxide radical *termini* and of comparable strength,[9a−c] hence ascertaining the dominant π-character of the spins. The temperature dependence of the weak signal observed at $g \approx 2$ for the open form $\mathbf{4o}^{2+}$ could not be recorded over a broad temperature range, due to the rapid decrease of the observed Curie-like law (Figure S18). The χT product does not vary with T above 4 K, thus following a pure Curie law for two isolated S = 1/2 spins in the accessible temperature range. This result suggests a very weak interaction between the two spin carriers not observable experimentally. If one refers to previous cited studies showing a singlet GS in nitronyl nitroxide radical based derivatives in the open form, the antiferromagnetic interaction of $\mathbf{4o}^{2+}$ with |ΔEST/k|< 1 K is expected to account for the observed behavior.[9a−c]

Thus, with this system, the spin density in the open state $\mathbf{4o}^{2+}$ is mainly located on the two amino-substituted carbon-rich ligands separated by a distance of 32.4 Å in the optimized structure, and delocalization is less important on the carbon-rich thiophene part preventing radical coupling in the oxidized state, in full agreement with the theoretical predictions. As expected, the observed exchange interaction between the spin carriers is small (<1 K). In the closed state $\mathbf{4c}^{2+}$, a fine balance in the electronic effect of the external and bridging carbon-rich

dx.doi.org/10.1021/ic5013044 | Inorg. Chem. 2014, 53, 8172−8188

ligand is operating. As attested by the theoretical calculations, the unpaired electrons are mostly localized on the RuC≡C-$C_6H_4NMe_2$ branches (0.65 e) and coupled by a polarization mechanism to provide a significant antiferromagnetic exchange interaction of −5 K. Overall, this photochromic system is comparable in magnetic exchange modulation to the organic system reported by Matsuda and Irie,[9a] the magnetic reading of the information (o/c) being possible only after redox "activation" of the reading process. Therefore, whereas photomodulation of exchange interaction has already been proved in purely organic systems incorporating DTE, the replacement of the organic radical by this redox-active organometallic spin source has several further advantages: (i) an increase of the complexity of the logic devices with the redox *stimuli* and (ii) a strong metal−carbon bond, which is maintained upon isomerization, in contrast to coordination complexes.[82]

7. Electrochemical Ring-Closing Mechanism. This electrochemical process has already been evidenced for several organic DTE-based systems mainly upon oxidation,[22−24] whereas some examples via reduction have also been reported.[25] The oxidative closing was reported to occur at high potential in those organic compounds as well as in some coordination adducts[36] (E > 1 V vs SCE). Therefore, it is remarkable that with **1o**−**3o** the isomerization process occurs at such low potentials (0.4−0.55 V) as recently observed for a series of photochromic DTE units with redox-active organometallic attachments.[43−46] At this stage, a further interesting point to address concerns the nature of the oxidized species of the open isomers involved in the ring-closing step. Indeed, two-electron waves are generally involved in the oxidation processes, and *a priori*, two limiting mechanistic pathways could be applied. The coupling step can occur either at the level of the mono-oxidized species (ECE mechanism) or at the bioxidized one (EEC mechanism) (Scheme 7). Surprisingly, despite the fact that this ring closing of organic DTE-based systems is a well-known phenomenon, the mechanistic pathway is more rarely explored.[23,24] In particular, Coudret and co-workers[23] provided strong evidence that the electrochemical ring closure of purely organic DTE involves the mono-oxidized species in the two-electron events (ECE mechanism).

In this context, cyclic voltammetry is a convenient tool for performing studies allowing the determination of the nature of such a mechanism and relevant kinetic data. More specifically, the use of the classical diagnostic criteria based on the variation of peak potential with scan rates and substrate concentration is a powerful method.[83,23] However, considering that **1o**−**3o** display slight to partial reversibility (depending on the nature of substituents), the "pure kinetic" conditions of the kinetic zone diagram do not apply in our case, preventing the use of that method.[84] Numerical simulation of the experimental data is another method to disclose the nature of the oxidized species involved in the ring-closure step. Thus, the simulated voltammograms were calculated at different scan rates through the DigiElch software,[76b] considering a coupling step involving the $\mathbf{1o}^{+}$−$\mathbf{3o}^{+}$ species in the ring-closing isomerization process on one hand and a mechanism involving the $\mathbf{1o}^{2+}$−$\mathbf{3o}^{2+}$ species on the other hand. The simulation parameters were set with experimental data (potential, k_s values, and concentration values) by considering that the charge-transfer coefficient, α, is equal to 0.5 and that the cyclization step is thermodynamically irreversible. The comparison of the experimental CV curves with the simulated ones allows distinguishing between the two possible pathways since the follow-up chemical reaction (closing) primarily exerts its influence on the chemical reversibility of the system. It results that the mechanism involving the $\mathbf{1o}^{2+}$−$\mathbf{3o}^{2+}$ species (Scheme 7, pathway B) matches well the experimental data, contrariwise to pathway A (Scheme 7), which failed in reproducing the characteristic patterns of the different experimental CVs (Figure S12). A representative example is displayed in Figure 11 with **3o**. In addition, the numerical simulations can give access to an accurate estimation of the kinetics of the following chemical reaction. Thus, the CVs also provide information on how the nature of the different substituents affects the kinetics of the ring-closure reaction. The kinetic coupling rate constants were found to be 0.5, 25, and 15 s^{-1} for compound **1o**, **2o**, and **3o**, respectively (Table 6). The lack of experimental kinetic data for such a process in the literature precludes any detailed comparison, but it is worth noting that this cyclization process is a rather slow process as compared to the photochemical opening or closing process.[85] However, in a purely organic perhydro-DTE system, the oxidation process was found to be chemically irreversible at scan rates up to 1000 V s^{-1}, meaning that the corresponding kinetic rate constant for the ring-closure process is greater than 10^4 s^{-1}.[24] Note that, if electrochemical closing could allow the formation of both the parallel and antiparallel isomers,[25] in our case only the antiparallel one can be obtained owing to steric constraints (*vide supra*).

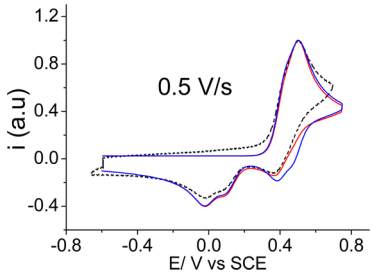

Figure 11. CV of **3o** ([c] = 10^{-3} mol L^{-1}, 0.2 mol L^{-1} Bu_4NPF_6, ν = 0.5 V s^{-1}) at a Pt electrode (black dashed line) and simulated CVs according to mechanistic pathway A (blue solid line) and mechanistic pathway B (red solid line). Currents were normalized.

From these results, it is revealed that the cyclization kinetics is obviously influenced by the electron density through the entire conjugated backbone. As stated in the theoretical part, the spin density on the C_{4DTE} carbon atoms of the two thiophene rings in the second oxidized state is in the order $\mathbf{3o}^{2+}$ > $\mathbf{2o}^{2+}$ > $\mathbf{1o}^{2+}$ ≫ $\mathbf{4o}^{2+}$. However, as also stated, the spin density is not the only parameter to consider. The activation energy and the relative stabilities of the dications are also involved. Associated with the energetic stabilization gained by the isomerization from $\mathbf{1o}^{2+}$−$\mathbf{3o}^{2+}$ to $\mathbf{1c}^{2+}$−$\mathbf{3c}^{2+}$ (energy ordering $\mathbf{2o}^{2+}$ ≫ $\mathbf{1o}^{2+}$ > $\mathbf{3o}^{2+}$), those two factors allow the rationalization of the observed kinetic trend of the order $\mathbf{2o}^{2+}$ > $\mathbf{3o}^{2+}$ > $\mathbf{1o}^{2+}$ and the inactivity of $\mathbf{4o}^{2+}$.

Previous examples in the literature show that the natures of the metal atoms and of the carbon-rich chain length are also of primary importance. Indeed, a closing reaction attributable to the same origin was observed for the related ruthenium species **A** with direct σ-bonds between the metals and the thiophene units of the DTE[45] or via acetylene[46] (**B**) or vinyl[44] linkers (**C**) (Chart 1). The case of the iron analogues deserves attention. For complex **D**, with direct σ-bonds between the metals and the

dx.doi.org/10.1021/ic5013044 | Inorg. Chem. 2014, 53, 8172−8188

Chart 1

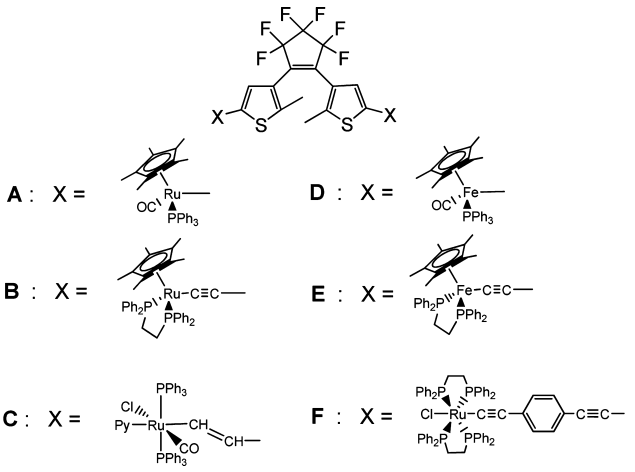

thienyl units, the closing is observed, whereas it is not present in **E**, with an acetylide spacer. DFT calculations on the double-oxidized open form of **B** and **E** show that the spin density is almost twice more important on the carbon atoms of interest for M = Ru than for M = Fe.[46] This is consistent with our results and with the usual larger ability for ruthenium complexes to accommodate the single electron on carbon-rich ligands. Finally, an additional phenylethynyl unit prevents the electrochemical closing in the ruthenium species,[86] showing that longer bridges lead to "dilution" of the spins and act against closing.

CONCLUSION

In summary, the perturbation of the DTE system by ruthenium units was used to reach three sophisticated light- and electro-triggered multifunctional switches featuring multicolor electrochromism and electrochemical cyclization. Significantly, these aforementioned systems present an efficient reversible photochromic activity along with an efficient low potential metal-promoted cyclization, in contrast with several other metallic systems.[36,44,45] In addition, with the help of spectroscopic (UV−vis−NIR−IR and EPR), electrochemical, and theoretical techniques, (i) we provide for the first time strong experimental evidence that cyclization occurs in the second oxidized state (EEC mechanism) along with a measure of the kinetic rate constants of the closing event in solution, and (ii) we show that with a slight modification of the ligand R remote from the DTE unit, we can manipulate the spin density on the DTE unit upon oxidation to control and to get a deeper understanding of the electrochemical cyclization process. Hence, these complexes provide an unprecedented experimental means to probe the efficiency of electronic (spin) delocalization between two *trans* carbon-rich ligands through a metal atom, in full agreement with the theoretical predictions. When the oxidative electrocyclization is prevented by the *trans* substituents, we can achieve a redox-triggered magnetic switch.

EXPERIMENTAL PART

General Comments. The reactions were achieved under an inert atmosphere, using Schlenk techniques. Solvents were freshly distilled under argon using standard procedures. The diethynyl-substituted dithienylethene,[87] Me_2N-*p*-C_6H_4-C≡CH,[88] and the ruthenium precursors [(dppe)$_2$RuCl](OTf),[89] [Cl(dppe)$_2$Ru=C=CH-p-C_6H_4-NO_2](OTf), and [Cl(dppe)$_2$Ru=C=CH-p-C_6H_5](OTf)[90] were prepared as previously reported. All the reactions and handling of the compounds were carried out in the dark. High-resolution mass spectra (HRMS) were recorded in Rennes at the CRMPO (Centre Régional de Mesures Physiques de l'Ouest) on a ZabSpecTOF (LSIMS at 4 kV) spectrometer. These large molecules inevitably contain inclusion solvents, precluding any satisfactory elemental analysis. Therefore, NMR spectra are provided in the Supporting Information (Figures S1−S6).

[Ph-C≡C-(dppe)$_2$Ru-C≡C-($C_{15}S_2F_6H_8$)-C≡C-Ru(dppe)$_2$-C≡C-Ph] (***1o***). In a Schlenk tube, [ClRu(dppe)$_2$=C=CH-Ph](OTf) (200 mg, 0.17 mol), $NaPF_6$ (57 mg, 0.34 mmol), and the diethynyl-substituted dithienylethene compound HC≡C-($C_{15}S_2F_6H_8$)-C≡CH (35 mg, 0.085 mmol) were pumped for 30 min. Then, dichloromethane (20 mL) comixed with triethylamine (0.12 mL, 0.85 mmol) was saturated with argon and transferred into the Schlenk tube. More triethylamine (0.12 mL, 0.85 mmol) was further added. The mixture was stirred for 4 days in the dark, and then the solvent was evaporated. The residue was dissolved in dichloromethane (20 mL), washed with degassed water (4 × 10 mL), and dried (Na_2SO_4). The solvent was evaporated, and the residue was washed with pentane (2 × 10 mL) and dried to obtain 170 mg of compound **1o** (83%) as a grayish-green solid. ^{31}P NMR (81 MHz, CD_2Cl_2, 297 K): δ 54.3 (s, PPh_2). ^{1}H NMR (200 MHz, $CDCl_3$, 297 K): δ 7.73−6.84 (m, 90 H, Ph), 6.23 (s, 2 H, H_{DTE}), 2.61 (m, 16 H, PCH_2CH_2P), 1.79 (s, 6 H, CH_3). ^{13}C NMR (75.5 MHz, CD_2Cl_2, 297 K): δ 137.17 and 136.72 (m, *ipso*-Ph (dppe)), 135.72 (C_{DTE}), 134.48 and 133.80 (o-Ph (dppe)), 130.44 (*ipso*-Ph (C≡C-Ph)), 129.77 (o-Ph (C≡C-Ph)), 128.87 and 128.55 (p-Ph (dppe)), 127.58 (m-Ph (C≡C-Ph)), 127.07 (m-Ph (dppe)), 124.12 and 123.96 (C_{DTE}), 123.09 (p-Ph (C≡C-Ph)), 117.61 (Ru-C≡C-Ph), 106.83 (Ru-C≡C-DTE), 31.44 (m, $|^1J_{PC} + {}^3J_{PC}|$ = 23 Hz, CH_2), 14.37 (CH_3). ^{19}F{^{1}H} NMR (188.3 MHz, CD_2Cl_2, 297 K): δ −110.181 (brd, 4F), −132.279 (brd, 2F). IR (KBr): ν 2052 cm^{-1} (C≡C). HR-MS FAB$^+$ (*m*/*z*): 2412.4166 ([M$^+$], calcd 2412.4254).

[O_2N-p-C_6H_4-C≡C-(dppe)$_2$Ru-C≡C-($C_{15}S_2F_6H_8$)-C≡C-Ru(dppe)$_2$-C≡C-p-C_6H_4-NO_2)] (***2o***). A 120 mg amount of compound **2o** (54%) as an orange powder was obtained from the above procedure, starting from compounds *trans*-[ClRu(dppe)$_2$=C=CH-p(C_6H_4)-NO_2](OTf) (201 mg, 0.16 mmol), HC≡C-($C_{15}S_2F_6H_8$)-C≡CH (34 mg, 0.082 mmol), $NaPF_6$ (55 mg, 0.33 mmol), triethylamine (0.24 mL, 1.7 mmol), and dichloromethane (20 mL). ^{31}P NMR (81 MHz, $CDCl_3$, 297 K): δ 54.3 (s, PPh_2). ^{1}H NMR (200 MHz, $CDCl_3$, 297 K): δ 8.02 (d, 4 H, $^3J_{HH}$ = 8.5 Hz, C_6H_4), 8.04−6.64 (m, 80 H, Ph), 6.66 (d, 4 H, $^3J_{HH}$ = 8.5 Hz, C_6H_4) 6.36 (s, 2 H, H_{DTE}), 2.62 (m, 16 H, PCH_2CH_2P), 1.86 (s, 6 H, CH_3). ^{13}C{^{1}H} NMR (75.5 MHz, CD_2Cl_2, 297 K): δ 136.23 (m, *ipso*-Ph (dppe)), 134.06 and 133.90 (o-Ph (dppe)), 129.87 (m-C_6H_4-NO_2), 129.04 and 128.89 (p-Ph (dppe)), 127.21 (m-Ph (dppe)), 124.99 and 124.15 (C_{DTE}), 123.34 (o-C_6H_4-NO_2), 118.73 (Ru-C≡C-$C_6H_4NO_2$), 106.44 (Ru-C≡C-DTE), 31.26 (m, $|^1J_{PC} + {}^3J_{PC}|$ = 23 Hz, CH_2), 14.08 (CH_3). ^{19}F{^{1}H} NMR (188.3 MHz, $CDCl_3$, 297 K): δ −109.920 (m, 4 F), −131.939 (m, 2 F). IR (KBr): ν 2043 cm^{-1} (C≡C). HR-MS FAB$^+$ (*m*/*z*): 2356.3788 ([M − C≡C-C_6H_4-NO_2] ($C_{131}H_{108}NO_2F_6P_8S_2$·102$Ru_2$)]$^+$, calcd 2356.3714)

[Cl-(dppe)$_2$Ru-C≡C-($C_{15}S_2F_6H_6$)-C≡C-Ru(dppe)$_2$-Cl] (***3o***). In a Schlenk tube, *trans*-[Cl(dppe)$_2$Ru](OTf) (172 mg, 0.16 mol) and HC≡C-($C_{15}S_2F_6H_8$)-C≡CH (33 mg, 0.08 mmol) were pumped for 30 min. Then, dichloromethane (20 mL) was transferred onto the solids. The mixture was stirred in the dark for 4 days before addition of triethylamine (0.2 mL, 3.2 mmol). After 30 min, the reacting solution was evaporated. The dichloromethane solution was washed with water (4 × 10 mL) and dried (Na_2SO_4), and the residue obtained after evaporation was washed with pentane (2 × 10 mL). A 100 mg amount of **1o** as a light green solid was recovered after drying under vacuum (55% yields). ^{31}P NMR (81 MHz, $CDCl_3$, 297 K): δ 50.3 (s, PPh_2). ^{1}H NMR (200 MHz, $CDCl_3$, 297 K): δ 7.55−6.97 (m, 80 H, Ph), 6.17 (s, 2 H, H_{DTE}), 2.69 (m, 16 H, CH_2), 1.78 (s, 6 H, CH_3). ^{13}C{^{1}H} NMR (75.5 MHz, C_6D_6, 297 K): δ 136.41 (m, *ipso*-Ph (dppe)), 135.36 (C_{DTE}), 135.09 and 134.07 (o-Ph (dppe)), 129.14 and 128.79 (p-Ph (dppe)), 127.23 (m-Ph (dppe)), 124.77 and 124.64 (C_{DTE}), 103.92 (Ru-C≡C), 30.97 (m, $|^1J_{PC} + {}^3J_{PC}|$ = 23 Hz, CH_2), 14.77 (CH_3). ^{19}F{^{1}H} NMR (188.3 MHz, CD_2Cl_2, 297 K): δ −110.144 (t, $^3J_{FF}$ = 6 Hz, 4F), −132.287 (quint, $^3J_{FF}$ = 6 Hz, 2 F). IR (KBr): ν 2055

dx.doi.org/10.1021/ic5013044 | *Inorg. Chem.* 2014, 53, 8172−8188

cm^{-1} (C≡C). HR-MS FAB$^+$ (m/z): 2261.2958 ([M − F]$^+$, calcd 2261.2865).

[Me_2N-p-C_6H_4-C≡C-(dppe)$_2$Ru-C≡C-($C_{15}S_2F_6H_8$)-C≡C-Ru-(dppe)$_2$-C≡C-p-C_6H_4-NMe_2)] ***(4o)***. In a Schlenk tube, compound **3o** (200 mg, 0.09 mmol), Me_2N-p-C_6H_4-C≡CH (51 mg, 0.36 mmol), and $NaPF_6$ (60 mg, 0.36 mmol) were pumped for 30 min. Then, dichloromethane (50 mL) comixed with triethylamine (0.13 mL, 0.9 mmol) was saturated with argon and transferred into the Schlenk tube. More triethylamine (0.13 mL, 0.9 mmol) was further added. The mixture was stirred for 6 days in the dark, and then the solvent was evaporated. The residue was dissolved in dichloromethane (40 mL), washed with aqueous potassium carbonate (3 × 15 mL) and with water (2 × 10 mL), and dried (Na_2SO_4). The solvent was evaporated, and the residue was washed with pentane (3 × 10 mL) and dried to obtain 150 mg of poorly soluble compound **4o** (67%) as a gray solid. ^{31}P NMR (81 MHz, CD_2Cl_2, 297 K): δ 54.3 (s, PPh_2). ^{1}H NMR (200 MHz, CD_2Cl_2, 297 K): δ 7.83−6.66 (m, 80 H, Ph), 6.85 (d, 4 H, $^3J_{HH}$ = 8.0 Hz, C_6H_4), 6.64 (d, 4 H, $^3J_{HH}$ = 8.0 Hz, C_6H_4), 6.30 (s, 2 H, H_{DTE}), 2.96 (s, 12 H, 2 NMe_2), 2.67 (m, 16 H, CH_2), 1.86 (s, 6 H, CH_3). ^{19}F{^{1}H} NMR (188.3 MHz, CD_2Cl_2, 297 K): δ −110.174 (br, 4F), −132.275 (br, 2F). IR (KBr): ν 2051 cm^{-1} (C≡C). HR-MS FAB$^+$ (m/z): 2498.4996 ([M$^+$], calcd 2498.5098).

[Ph_2C=C=C=(dppe)$_2$Ru-C≡C-($C_{15}S_2F_6H_8$)-C≡C−Ru(dppe)$_2$=C=C=CPh_2)][PF_6]$_2$ ***(5o)***. In a Schlenk tube, compound **3o** (141 mg, 0.062 mmol), propargylic alcohol $Ph_2C(OH)C≡CH$ (35 mg, 0.167 mmol), and $NaPF_6$ (42 mg, 0.247 mmol) were dried under reduced pressure for 30 min. After addition of CH_2Cl_2 (30 mL), the reaction was allowed to stir at room temperature for 6 days. The reaction mixture was filtered, washed with water (3 × 10 mL), and dried over sodium sulfate. The solvent was removed *in vacuo*, and the crude solid washed with Et_2O (3 × 10 mL). Crystallizations in a mixture of CH_2Cl_2−pentane led to **5o** as a dark blue solid (164 mg; 50%). ^{31}P NMR (81 MHz, CD_2Cl_2, 297 K): δ 44.7 (s, PPh_2), −144.2 (sep, $^1J_{PF}$ = 710 Hz, PF_6). ^{1}H NMR (200 MHz, CD_2Cl_2, 297 K): δ 7.68−6.78 (m, 100H, Ph), 6.55 (s, 2H, H_{DTE}); 2.88 (m, 16H, P(CH_2)$_2$P); 2.01 (s, 6H, CH_3). ^{13}C NMR (75.5 MHz, C_6D_6, 297 K): δ 315.70 (quint., $^2J_{PC}$ = 13 Hz), 206.40 (Ru=C=C), 162.60 (Ru=C=C=C), 144.17, 139.84, 133.47, 133.21, 130.93, 130.70, 130.30, 129.09, 128.45, 128.05, 126.05, and 124.68 (C_{DTE}), 29.11 (m, $|^1J_{PC} + {}^3J_{PC}|$ = 23 Hz, CH_2], CH_2), 14.65 (CH_3). IR (KBr): ν 2071 cm^{-1} (C≡C), 1924 (=C=C=C), 838 (PF). HR-MS FAB$^+$ (m/z): 2735.4824 ([(M^{2+}, PF_6^-)$^+$], calcd 2735.46785).

[($C_6H_4NMe_2$)-C≡C-(dppe)$_2$Ru-C≡C-(C_6H_5)] ***(6)***. In a Schlenk tube, *trans*-[ClRu(dppe)$_2$=C=CH-Ph](OTf) (200 mg, 0.17 mmol), Me_2N-p-C_6H_4-C≡CH (29.40 mg, 0.21 mmol), and $NaPF_6$ (56.8 mg, 0.34 mmol) were pumped for 30 min. Then, dichloromethane (20 mL) comixed with triethylamine (0.24 mL, 1.7 mmol) was saturated with argon and transferred into the Schlenk tube. The mixture was stirred for 1 day, and then the solvent was evaporated. The residue was solved in dichloromethane (40 mL), washed with aqueous potassium carbonate (3 × 15 mL), then with fresh water (2 × 10 mL), and dried (Mg_2SO_4). The solvent was evaporated, and the residue was washed with pentane (2 × 10 mL) and dried to obtain 160 mg of compound **15** (82.%), as a light yellow-green solid. ^{31}P{^{1}H} NMR (81 MHz, $CDCl_3$, 297 K): δ 55.2 (s, PPh_2). ^{1}H NMR (200 MHz, $CDCl_3$, 297 K): δ 7.58−6.61 (m, 89 H, Ph), 2.96 (s, 6 H, NMe_2), 2.64 (m, 8 H, PCH_2CH_2P). ^{13}C NMR (75.5 MHz, CD_2Cl_2, 297 K): δ 147.21 (*ipso*-C_6H_4-NMe_2), 137.46 (m, *ipso*-Ph (dppe)), 134.36 and 134.21 (o-Ph (dppe)), 130.70 (*ipso*-Ph (C≡C-Ph)), 130.49 (o-Ph (C≡C-Ph)), 129.90 (m-C_6H_4-NMe_2), 128.49 (p-Ph (dppe)), 127.41 (m-Ph (C≡C-Ph)), 126.90 (m-Ph (dppe)), 122.70 (p-Ph (C≡C-Ph)), 119.95 (p-C_6H_4-NMe_2), 116.20 and 116.12 (Ru-C≡C-$C_6H_4NMe_2$ and Ru-C≡C-Ph), 112.43 (o-C_6H_4-NMe_2), 40.67 (NMe_2), 31.46 (m, PCH_2CH_2P, $|^1J_{PC} + {}^3J_{PC}$ = 23 Hzl, CH_2). IR (KBr): ν 2061 cm^{-1} (C≡C). HR-MS FAB$^+$ (m/z): 1143.2966 ([M$^+$], calcd 1143.2955).

Isomerization Studies. UV−vis irradiation was performed with an LS series light source from ABET Technologies, Inc. (150 W xenon lamp), with single-wavelength light filters "350FS 10−25", "450FS 20−25", "650FS 10−25", and "750FS 40−25". UV−vis−NIR spectra were recorded with a Cary 5000 apparatus.

[(C_6H_5)-C≡C-(dppe)$_2$Ru-C≡C-($C_{15}S_2F_6H_8$)-C≡C−Ru(dppe)$_2$-C≡C-(C_6H_5)] ***(1c)***. ^{31}P NMR (81 MHz, C_6D_6, 297 K): δ 54.3 (s, PPh_2). ^{1}H NMR (200 MHz, C_6D_6, 297 K): δ 7.94−6.94 (m, 90 H, Ph), 5.67 (s, 2 H, ArH), 2.64 (s, 6 H, $ArCH_3$), 2.46 (m, 16 H, PCH_2CH_2P). IR (KBr): ν 2012 cm^{-1} (C≡C).

[($C_6H_4NO_2$)-C≡C-(dppe)$_2$Ru-C≡C-($C_{15}S_2F_6H_8$)-C≡C-Ru(dppe)$_2$-C≡C($C_6H_4NO_2$)] ***(2c)***. ^{31}P NMR (81 MHz, C_6D_6, 297 K): δ 53.8 (s, PPh_2). ^{1}H NMR (200 MHz, C_6D_6, 297 K): δ 8.10−6.83 (m, 88 H, Ph), 5.80 (s, 2 H, ArH), 2.63 (s, 6 H, $ArCH_3$), 2.41 (m, 16 H, PCH_2CH_2P). IR (KBr): ν 2019 cm^{-1} (C≡C).

[Cl-(dppe)$_2$Ru-C≡C-($C_{15}S_2F_6H_8$)-C≡C-Ru(dppe)$_2$-Cl] ***(3c)***. ^{31}P NMR (81 MHz, C_6D_6, 297 K): δ 49.5 (s, PPh_2). ^{1}H NMR (200 MHz, C_6D_6, 297 K): δ 7.84−6.95 (m, 80 H, Ph), 5.43 (s, 2 H, ArH), 2.61 (s, 6 H, $ArCH_3$), 2.52 (m, 16 H, PCH_2CH_2P). IR (KBr): ν 2009 cm^{-1} (C≡C).

[($C_6H_4NMe_2$)-C≡C-(dppe)$_2$Ru-C≡C-($C_{15}S_2F_6H_8$)-C≡C-Ru(dppe)$_2$-C≡C-($C_6H_4NMe_2$)] ***(4c)***. ^{31}P NMR (81 MHz, C_6D_6, 297 K): δ 54.4 (s, PPh_2). ^{1}H NMR (200 MHz, C_6D_6, 297 K): δ 8.05−6.75 (m, 88 H, Ph), 5.66 (s, 2 H, ArH), 2.66 (s, 6 H, $ArCH_3$), 2.61 (s, 12 H, 2 NMe_2), 2.50 (m, 16 H, PCH_2CH_2P). IR (KBr): ν 2009 cm^{-1} (C≡C).

Electrochemistry. Electrochemical studies were carried out under argon using an instrument consisting of a Tacussel GSTP4 programmer and a home-built potentiostat equipped with a positive feedback compensation device (CH_2Cl_2, 0.2 mol L^{-1} Bu_4NPF_6).[91] The voltammograms were recorded with a 310 Nicolet oscilloscope. The working electrode was a Pt disk, the counter electrode was a Pt wire, and a SCE electrode was used as a reference electrode. After each series of experiments, ferrocene and decamethylferrocene were added to the electrolyte to serve as internal probes.[92]

Macroelectrolyses under an argon atmosphere were performed at controlled potential with a three-electrode configuration in a two-compartment cell. A Pt plate (3 cm^2) was used as a working electrode, a Pt disk (1 mm diameter) was used as a secondary working electrode, an SCE electrode with an extension (CH_2Cl_2, 0.2 mol L^{-1} Bu_4NPF_6) served as a reference electrode, and a Pt grid was the counter electrode. Experiments were performed with an EGG PAR-173 potentiostat and an EGG PAR-175 universal programmer equipped with an EGG PAR-179 digital coulometer. For each macroscale electrolysis, a dilute CH_2Cl_2 solution (ca. 10^{-3} mol L^{-1}) of the compounds was prepared with Bu_4NPF_6 (0.2 mol L^{-1}) as the supporting electrolyte. The applied oxidation potentials were calibrated upon performing cyclic voltammetry before electrolysis. By recording CVs, the secondary Pt electrode was used to control the consumption of the starting materials throughout the bulk electrolysis. Electrolyses were stopped after the current was dropped to less than 10% of its initial value. All the reactions and handling of the compound were carried out in the dark.

UV−vis−NIR spectroelectrochemistry (SEC) experiments were performed in CH_2Cl_2 at 20 °C, under argon, with a homemade OTTLE cell, path length = 1 mm, using a Varian CARY 5000 spectrometer and an EG&G PAR model 362 potentiostat. A Pt mesh was used as the working electrode, a Pt wire as the counter electrode, and an Ag wire as a pseudoreference electrode. The electrodes were arranged in the cell such that the Pt mesh was in the optical path of the quartz cuvette. The anhydrous freeze−pump−thaw degassed sample−electrolyte solution (0.2 mol L^{-1} Bu_4NPF_6) was cannula-transferred under argon into the cell, which was previously thoroughly deoxygenated. The oxidation potentials were calibrated upon performing cyclic voltammetry before electrolysis. Isosbestic points observed along the whole experiment show the clean conversion processes.

Numerical simulations of the voltammograms were performed with the DigiElch simulation software (Elchsoft),[76b] using the default numerical options with the assumption of a planar diffusion and a Butler−Volmer law for the electron transfer. The charge-transfer coefficient, α, was taken as 0.5. The k values (apparent heterogeneous electronic kinetic rate constants) were determined from peak-to-peak separations in the reversible systems, assuming D = 10^{-5} cm^2 s^{-1}.

EPR Spectroscopy. Experiments were performed on an ESP300E (Bruker) spectrometer operating at the X-band (9.3−9.8 GHz) and equipped with a rectangular TE102 resonator. Variable-temperature

dx.doi.org/10.1021/ic5013044 | Inorg. Chem. 2014, 53, 8172−8188

measurements were performed with the help of an ESR900 (Oxford Instruments) continuous flow He cryostat. Samples were degassed before measurements, and temperature was measured with a thermocouple (AuFe/Chromel) introduced inside the EPR tube.

Theoretical Calculations. Density functional theory calculations were performed using the Amsterdam Density Functional package (ADF 2013.01)[93] on simplified structures of **1**−**4o**/**c**$^{0/2+}$ in which hydrogen atoms replace the phenyl groups of dppe ligands. The singlet and triplet states were considered for dications, i.e., closed-shell low-spin singlet state (LS), high-spin triplet state (HS), and open-shell singlet spin state (two unpaired antiparallel electrons, BS). The latter cannot be calculated directly by DFT means due to the monodeterminantal nature of this methodology, but it was shown by Noodleman et al. that the broken-symmetry approach (BS) allows the calculation of its total energy.[94] The geometries were optimized without symmetry constraints (C_1 symmetry). For BS calculations, the geometry of the triplet corresponding state was used and the protocol detailed in the ADF manual was applied. Electron correlation was treated within the local density approximation (LDA) in the Vosko−Wilk−Nusair parametrization.[95] The nonlocal corrections of Becke and Perdew (BP86) were added to the exchange and correlation energies, respectively.[96] The analytical gradient method implemented by Verluis and Ziegler was used.[97] The standard ADF TZP basis set was used, i.e., triple-ξ STO basis set for the valence core augmented with a 3d polarization function for C and P. Orbitals up to 1s, 2p, and 4p were kept frozen for C, P, and Ru, respectively.[98] Single-point energy calculations were performed using the B3LYP functional with an all-electron TZP atomic basis set. The bonding energies and Cartesian coordinates of each structure are given in Table S5. Because of the size of the molecules and thus of computational limits, frequency analysis were not performed, but the geometry optimization convergence criteria were more drastic than default ones (energy change <0.0005 hartree, atomic position displacement <0.005 Å).

The excitation energies and oscillator strengths were calculated following the procedure described by van Gisbergen and co-wokers.[99] In that case, the functional used was PBE.[100]

■ ASSOCIATED CONTENT

Supporting Information

IR, UV/vis/NIR, and EPR spectra, IR spectroelectrochemical studies, isomerization studies, voltammetric scans and simulations, and quantum chemical results (main structural data, relative energies, atomic spin densities, and Cartesian coordinates of all calculated systems). This material is available free of charge via the Internet at http://pubs.acs.org.

■ AUTHOR INFORMATION

Corresponding Authors

*E-mail: corinne.lagrost@univ-rennes1.fr (C.L.).
*E-mail: karine.costuas@univ-rennes1.fr (K.C.).
*E-mail: stephane.rigaut@univ-rennes1.fr (S.R.).

Notes

The authors declare no competing financial interest.

■ ACKNOWLEDGMENTS

The authors thank the CNRS, the University of Rennes 1, the ANR (No. ANR-09-JCJC-0025), and the AUF for a grant to C.M.N. This work was also performed using HPC resources from GENCI-CINES and GENCI-IDRIS (Grants 2013-80649 and 2014-80649).

■ REFERENCES

(1) Richard Feynman's original lecture "plenty of room at the bottom": www.its.caltech.edu/~feynman.

(2) Aviram, A.; Ratner, M. A. *Chem. Phys. Lett.* **1974**, *29*, 277. Carroll, R. L.; Gorman, C. B. *Angew. Chem.* **2002**, *41*, 437. Nitzan, J. A.; Ratner, M. A. *Science* **2003**, *300*, 1384. McCreery, R. L. *Chem. Mater.* **2004**, *16*, 4477. Joachim, C.; Ratner, M. A. *Proc. Natl. Acad. Sci. U.S.A.* **2005**, *102*, 8801. Metzger, R. M. *J. Mater. Chem.* **2008**, *18*, 4364. Choi, S. H.; Kim, B.-S.; Frisbie, C. D. *Science* **2008**, *320*, 1382.

(3) Dürr, H.; Bouas-Laurent, H. *Photochromism: Molecules and Systems*; Elsevier, Amsterdam, 1990. Special issue on "Photochromism: Memories and Switches": *Chem. Rev.* **2000**, *100*, 1683. *Molecular Switches*; Feringa, B. L., Ed.; Wiley-VCH: Weinheim, 2001. Crano, J. C.; Guglielmetti, R. *Organic Photochromic and Thermochromic Compounds*, Vol. 1; Plenum Press: New York, 1999.

(4) Irie, M. *Chem. Rev.* **2000**, *100*, 1685.

(5) Kuderna, T.; Katsoni, N.; Browne, W. R.; Feringa, B. L. *J. Mater. Chem.* **2009**, *19*, 7168. Wang, M.-S.; Xu, G.; Zhang, Z.-J.; Guo, G.-C. *Chem. Commun.* **2010**, *46*, 361. Tian, H.; Wang, S. *Chem. Commun.* **2007**, 781. Yildiz, I.; Deniz, E.; Raymo, F. R. *Chem. Soc. Rev.* **2009**, *38*, 1859. Balzani, V.; Credi, A.; Venturi, M. *Chem.—Eur. J.* **2008**, *14*, 26.

(6) Carella, A.; Coudret, C.; Guirado, G.; Rapenne, G.; Vives, G.; Launay, J.-P. *Dalton Trans.* **2008**, 177.

(7) Russew, M.-M.; Hecht, S. *Adv. Mater.* **2010**, *22*, 3348. Klajn, R.; Stoddart, J. F.; Grzybowski, B. A. *Chem. Soc. Rev.* **2010**, *39*, 2203. Orgiu, E.; Samori, P. *Adv. Mater.* **2014**, *26*, 1827.

(8) Kume, S.; Nishihara, H. *Dalton Trans.* **2008**, 3260.

(9) (a) Matsuda, K.; Irie, M. *J. Am. Chem. Soc.* **2000**, *122*, 8309. (b) Tanifuji, N.; Irie, M.; Matsuda, K. *J. Am. Chem. Soc.* **2005**, *127*, 13344−13353. (c) Takayama, K.; Matsuda, K.; Irie, M. *Chem.—Eur. J.* **2003**, *9*, 5605. (d) Okudo, M.; Enoùoto, W. M.; Kojima, N. *Synth. Met.* **2005**, *152*, 461. (e) Sénéchal-David, K.; Zaman, N.; Walko, M.; Halza, E.; Riviere, E.; Guillot, R.; Feringa, B. L.; Boillot, M.-L *Dalton Trans.* **2008**, 1932. (f) Shiga, T.; Miyasaka, H.; Yamashita, M.; Morimoto, M.; Irie, M. *Dalton Trans.* **2011**, *40*, 2275−2282. (g) Hehei, M.; Susuki, Y.; Mimura, N.; Kera, Y.; Oshio, H. *Chem.—Eur. J.* **2013**, *19*, 6946. (h) Milek, M.; Heinemann, F. W.; Khusniyarov, M. M. *Inorg. Chem.* **2013**, *52*, 11585.

(10) Kronemeijer, A. J.; Akkerman, H. B.; Kudernac, T.; van Wees, B. J.; Feringa, B. L.; Blom, P. W. M.; de Boer, B. *Adv. Mater.* **2008**, *20*, 1467. Ikeda, M.; Tanifuji, N.; Yamaguchi, H.; Irie, M.; Matsuda, K. *Chem. Commun.* **2007**, 1355. He, Y.; Yamamoto, Y.; Jin, W.; Fukushima, T.; Saeki, A.; Seki, S.; Ishii, N.; Aida, T. *Adv. Mater.* **2010**, *22*, 829. Uchida, K.; Yamanoi, Y.; Yonezawa, T.; Nishihara, H. *J. Am. Chem. Soc.* **2011**, *133*, 9239. Jia, C.; Wang, J.; Yao, C.; Cao, Y.; Zhong, Y.; Liu, Z.; Liu, Z.; Guo, X. *Angew. Chem., Int. Ed.* **2013**, *52*, 8666. Kim, Y.; Hellmuth, T. J.; Sysoiev, D.; Pauly, F.; Pietsch, T.; Wolf, J.; Erbe, A.; Huhn, T.; Groth, U.; Steiner, U. E.; Scheer, E. *Nano Lett.* **2012**, *12*, 3736. Roldan, D.; Kaliginedi, V.; Cobo, S.; Kolivoska, V.; Bucher, C.; Hong, W.; Royal, G.; Wandlowski, T. J. *J. Am. Chem. Soc.* **2013**, *135*, 5974.

(11) Meng, F.; Hervault, Y.-M.; Norel, L.; Costuas, K.; Van Dyck, C.; Geskin, V.; Cornil, J.; Hng, H. H.; Rigaut, S.; Chen, X. *Chem. Sci.* **2012**, *3*, 3113. Meng, F.; Hervault, Y.-M.; Shao, Q.; Hu, B.; Norel, L.; Rigaut, S.; Chen, X. *Nat. Commun.* **2014**, *5:3023*, DOI: 10.1038/ncomms4023.

(12) Hayasaka, H.; Miyashita, T.; Tamura, K.; Akagi, K. *Adv. Funct. Mater.* **2010**, *20*, 1243.

(13) Aubert, V.; Guerchais, V.; Ishow, E.; Hoang-Thi, K.; Ledoux, I.; Nakatani, K.; Le Bozec, H. *Angew. Chem., Int. Ed.* **2008**, *47*, 577. Wu, T.; Barker, M.; Arafeh, K. M.; Boyer, J.-C.; Carling, C.-J.; Branda, N. *Angew. Chem., Int. Ed.* **2013**, *52*, 11106. Castellenos, S.; Vieira, A. A.; Illescas, B. M.; Sacchetti, V.; Shubert, C.; Moreno, J.; Guldi, D. M.; Hecht, S.; Martin, N. *Angew. Chem., Int. Ed.* **2013**, *52*, 13985. Hayasaka, H.; Miyashita, T.; Kakayama, M.; Kuwada, K.; Akagi, K. *J. Am. Chem. Soc.* **2012**, *134*, 3758. Pace, T. C. S.; Müller, V.; Li, S.; Lincoln, P.; Andréasson, J. *Angew. Chem., Int. Ed.* **2013**, *52*, 4393. Wu, T.; Bohne, C.; Branda, N. R. *Angew. Chem., Int. Ed.* **2012**, *51*, 2741.

(14) Morimoto, M.; Irie, M. *J. Am. Chem. Soc.* **2010**, *132*, 14172−14178.

(15) Shallcross, R. C.; Körner, P. O.; Maibach, E.; Köhnen, A.; Meerholz, K. *Adv. Mater.* **2013**, *25*, 4807. Zhang, Z.; Liu, X.; Li, Z.; Chen, Z.; Zhao, F.; Zhang, F.; Tung, C.-H. *Adv. Funct. Mater.* **2008**, *18*, 302. Orgiu, E.; Crivillers, N.; Herderqq, M.; Grubert, L.; Pätzel,

M.; Frish, J.; Pavlica, E.; Duong, D. T.; Bratina, G.; Salleo, A.; Koch, N.; Hecht, S.; Samori, P. *Nat. Chem.* **2012**, *4*, 675.
(16) Patre, A.; Metivier, R.; Brisset, F.; Nakatani, K. *Chem. Commun.* **2012**, *48*, 2489.
(17) Che, S.; Guo, Z.; Zhu, S.; Shi, W.-e; Zhu, W. *ACS Appl. Mater. Interfaces* **2013**, *5*, 5623.
(18) Zhang, J.; Jin, J.; Zou, L.; Tian, H. *Chem. Commun.* **2013**, *49*, 9926.
(19) Al-Atar, U.; Fernandes, R.; Johnsen, B.; Baillie, D.; Branda, N. R. *J. Am. Chem. Soc.* **2009**, *131*, 15966.
(20) Mori, K.; Ishibashi, Y.; Matsuda, H.; Ito, S.; Nagasawa, Y.; Nakagawa, H.; Uchida, K.; Yokojima, S.; Nakamura, S.; Irie, M.; Miyasaka, H. *J. Am. Chem. Soc.* **2011**, *133*, 2621. Boyer, J.-C.; Carling, C.-J.; Gates, B. D.; Branda, N. R. *J. Am. Chem. Soc.* **2010**, *132*, 15766.
(21) Higashiguchi, K.; Matsuda, K.; Irie, M. *Angew. Chem., Int. Ed.* **2003**, *42*, 3537. Liu, H.; Chen, Y. *J. Mater. Chem.* **2011**, *21*, 1246. Li, B.; Wu, Y.-H.; Wen, H. M.; Shi, L.-X.; Chen, Z.-N. *Inorg. Chem.* **2012**, *51*, 1933.
(22) Peters, A.; Branda, N. *J. Am. Chem. Soc.* **2003**, *125*, 3404. Peters, A.; Branda, N. *Chem. Commun.* **2003**, *125*, 954. Moriyama, Y.; Matsuda, K.; Tanifuji, N.; Irie, S.; Irie, M. *Org. Lett.* **2005**, *7*, 3315.
(23) Guirado, G.; Coudret, C.; Hliwa, M.; Launay, J.-P. *J. Phys. Chem. B* **2005**, *109*, 17445.
(24) Browne, W. R.; de Jong, J. J. P.; Kudernac, T.; Walko, M.; Lucas, L. N.; Uchida, K.; van Esch, J. H.; Feringa, N. L. *Chem.—Eur. J.* **2005**, *11*, 6414. Browne, W. R.; de Jong, J. J. P.; Kudernac, T.; Walko, M.; Lucas, L. N.; Uchida, K.; van Esch, J. H.; Feringa, N. L. *Chem.—Eur. J.* **2005**, *11*, 6430.
(25) Gorodetsky, B.; Samachetty, H. D.; Donkers, R. L.; Workentin, M. S.; Branda, N. R. *Angew. Chem., Int. Ed.* **2004**, *43*, 2813. Leaustic, A.; Anxolabéhère-Mallart, E.; Maurel, F.; Midelton, S.; Guillot, R.; Metivier, R.; Nakatani, K.; Yu, P. *Chem.—Eur. J.* **2011**, *17*, 2246.
(26) One system combines both events; see: Gorodetsky, B.; Branda, N. R. *Adv. Funct. Mater.* **2007**, *17*, 786.
(27) Baron, R.; Onopriyenko, A.; Lioubasheviski, O.; Willner, I.; Wang, S.; Tian, H. *Chem. Commun.* **2006**, 2147. Bowne, W. R.; Kudernac, T.; Katsonis, N.; Areephong, J.; Hjelm, J.; Feringa, B. L. *J. Phys. Chem. C* **2008**, *112*, 1183.
(28) Nakashima, Y.; Kajiki, Y.; Fukumoto, S.; Tagushi, M.; Nagao, S.; Hirota, S.; Kawai, T. *J. Am. Chem. Soc.* **2012**, *134*, 19877.
(29) Samoc, M.; Gauthier, N.; Cifuentes, M. P.; Paul, F.; Lapinte, C.; Humphrey, M. G. *Angew. Chem., Int. Ed.* **2006**, *45*, 7376.
(30) Guerchais, V.; Ordronneau, L.; Le Bozec, H. *Coord. Chem. Rev.* **2010**, *254*, 2533.
(31) Ko, C. C.; Yam, V. W.-W. *J. Mater. Chem.* **2010**, *20*, 2063.
(32) Muraoka, T.; Kinbara, K.; Aida, T. *Nature* **2006**, *440*, 512.
(33) Venkataramani, S.; Jana, U.; Dommaschk, M.; Sönnichsen, F. D.; Tuczek, F.; Herges, R. *Science* **2011**, *331*, 445.
(34) Fernandez-Acebes, A.; Lehn, J.-M. *Chem.—Eur. J.* **1999**, *5*, 3285.
(35) Zhu, L.; Zhang, D.; Qu, D.; Wang, Q.; Ma, X.; Tian, H. *Chem. Commun.* **2010**, *46*, 2587.
(36) Zhong, Y.-W.; Vila, N.; Henderson, J. C.; Flores-Torres, S.; Abruña, H. D. *Inorg. Chem.* **2007**, *46*, 10470. Zhong, Y.-W.; Vila, N.; Henderson, J. C.; Abruña, H. D. *Inorg. Chem.* **2009**, *48*, 991.
(37) Roberts, M. N.; Carling, C.-J.; Nagle, J. K.; Branda, N. R.; Wolf, M. O. *J. Am. Chem. Soc.* **2009**, *131*, 16644. Roberts, M. N.; Nagle, J. K.; Finden, J. G.; Branda, N. R.; Wolf, M. O. *Inorg. Chem.* **2009**, *48*, 19.
(38) Wong, H.-L.; Tao, C.-H.; Zhu, N.; Yam, V. W.-W. *Inorg. Chem.* **2011**, *50*, 471. Lee, P. H.-OM.; Ko, C. C.; Zhu, N.; Yam, V. W.-W. *J. Am. Chem. Soc.* **2007**, *129*, 6058. Ko, C. C.; Kwok, W.-M.; Yam, V. W.-W.; Phillips, D. L. *Chem.—Eur. J.* **2006**, *12*, 5840.
(39) Jukes, R. T. F.; Adamo, V.; Hartl, F.; Belser, P.; De Cola, L. *Inorg. Chem.* **2004**, *43*, 2779. Indelli, M. T.; Carli, S.; Ghirotti, M.; Chiorboli, C.; Ravaglia, M.; Garavelli, M.; Scandola, F. *J. Am. Chem. Soc.* **2009**, *130*, 7286.
(40) Zhang, J.; Riskin, M.; Tel-Vered, R.; Tian, H.; Willner, I. *Langmuir* **2011**, *27*, 1380.
(41) Fraysse, S.; Coudret, C.; Launay, J.-P. *Eur. J. Inorg. Chem.* **2000**, 1581. Guirado, G.; Coudret, C.; Launay, J.-P. *J. Phys. Chem. B* **2007**, *111*, 2770.
(42) Akita, M. *Organometallics* **2011**, *30*, 43.
(43) (a) Liu, Y.; Lagrost, C.; Costuas, K.; Tchouar, N.; Le Bozec, H.; Rigaut, S. *Chem. Commun.* **2008**, 6117. (b) Hervault, Y.-M.; Ndiaye, C. M.; Norel, L.; Lagrost, C.; Rigaut, S. *Org. Lett.* **2012**, *14*, 4454.
(44) Lin, Y.; Yuan, J.; Hu, M.; Chen, J.; Yin, J.; Jin, S.; Liu, S. H. *Organometallics* **2009**, *28*, 6402. Lin, Y.; Yuan, J.; Hu, M.; Li, Z.; Yu, G.-A.; Liu, S. H. *Organometallics* **2010**, *29*, 2808.
(45) Motoyama, K.; Koike, T.; Akita, M. *Chem. Commun.* **2008**, 5812.
(46) Tanaka, Y.; Ishisaka, T.; Inagaki, A.; Koike, T.; Lapinte, C.; Akita, M. *Chem.—Eur. J.* **2010**, *16*, 4762. Tanake, Y.; Inagaki, A.; Akita, M. *Chem. Commun.* **2007**, 1169.
(47) Wen, H.-M.; Li, B.; Wang, J. Y.; Shi, L.-X.; Chen, C.-N.; Chen, Z.-N. *Organometallics* **2013**, *32*, 1759. Li, B.; Wang, J. Y.; Wen, H.-M.; Shi, L.-X.; Chen, Z.-N. *J. Am. Chem. Soc.* **2012**, *134*, 16059.
(48) Mitchell, R. H.; Brkic, Z.; Sauro, V. A.; Berg, D. J. *J. Am. Chem. Soc.* **2003**, *125*, 7581. Muratsugu, S.; Kume, S.; Nishihara, H. *J. Am. Chem. Soc.* **2008**, *130*, 7204.
(49) Gherab, K. N.; Gatri, R.; Hank, Z.; Dick, B.; Kutta, R.-J.; Winter, R.; Luc, J.; Sahraoui, B.; Fillaut, J.-L. *J. Mater. Chem.* **2010**, *20*, 2858.
(50) He, B.; Wenger, O. S. *Inorg. Chem.* **2012**, *51*, 4335.
(51) Hasewaga, Y.; Nakagawa, T.; Kawai, T. *Coord. Chem. Rev.* **2010**, *254*, 2643.
(52) (a) Costuas, K.; Rigaut, S. *Dalton Trans.* **2011**, *40*, 5643. (b) Aguirre-Etchevery, P.; O'Hare, D. *Chem. Rev.* **2010**, *110*, 4839. (c) Low, P. J.; Brown, N. J. *J. Cluster Sci.* **2010**, *21*, 235. (d) Záliš, S.; Winter, R. F.; Kaim, W. *Coord. Chem. Rev.* **2010**, *254*, 1383. (e) Ren, T. *Organometallics* **2005**, *24*, 4854. (f) Akita, M.; Koike, T. *Dalton Trans.* **2008**, 3523. (g) Bruce, M. I.; Low, P. J. *Adv. Organomet. Chem.* **2004**, *50*, 179. (h) Szafert, S.; Gladysz, J. A. *Chem. Rev.* **2003**, *103*, 4175. (i) Venkatesan, K.; Blacque, O.; Berke, H. *Dalton Trans.* **2007**, 1091.
(53) Rigaut, S. *Dalton Trans.* **2013**, *42*, 15859.
(54) Paul, F.; Costuas, K.; Ledoux, I.; Deveau, S.; Zyss, J.; Halet, J.-F.; Lapinte, C. *Organometallics* **2002**, *21*, 5229. Cifuentes, M. P.; Humphrey, M. G.; Morrall, J. P.; Samoc, M.; Paul, F.; Lapinte, C.; Roisnel, T. *Organometallics* **2005**, *24*, 4280.
(55) Di Piazza, E.; Norel, L.; Costuas, K.; Bourdolle, A.; Maury, O.; Rigaut, S. *J. Am. Chem. Soc.* **2011**, *133*, 6174. Norel, L.; Di Piazza, E.; Feng, M. A.; Vacher, A.; He, X.; Roisnel,T.; Maury, O.; Rigaut, S. *Organometallics*, DOI: 10.1021/om500059d. Wong, K. M.-C.; Lam, S. C.-F.; Ko, C.-C.; Zhu, N.; Yam, V. W.-W.; Roué, S.; Lapinte, C.; Fathallah, S.; Costuas, K.; Kahlal, S.; Halet, J.-F. *Inorg. Chem.* **2003**, *42*, 7086.
(56) Norel, L.; Bernot, K.; Feng, M.; Roisnel, T.; Caneschi, A.; Sessoli, R.; Rigaut, S. *Chem. Commun.* **2012**, *48*, 3948. (b) Norel, L.; Min, F.; Bernot, K.; Roisnel, T.; Guizouarn, T.; Costuas, K.; Rigaut, S. *Inorg. Chem.* **2014**, *53*, 2361.
(57) Qi, H.; Gupta, A.; Noll, B. C.; Snider, G. L.; Lu, Y.; Lent, C.; Fehlner, T. P. *J. Am. Chem. Soc.* **2005**, *127*, 15218.
(58) Zhu, Y.; Clot, O.; Wolf, M. O.; Yap, G. P. A. *J. Am. Chem. Soc.* **1998**, *120*, 1812. Xu, G.-L.; Crutchley, R. J.; De Rosa, M. C.; Pan, Q.-J.; Zhang, H.-X.; Wang, X.; Ren, T. *J. Am. Chem. Soc.* **2005**, *127*, 13354. Rigaut, S.; Costuas, K.; Touchard, D.; Saillard, J.-Y.; Golhen, S.; Dixneuf, P. H. *J. Am. Chem. Soc.* **2004**, *126*, 4072.
(59) Ying, J.-W.; Po-Chun Liu, I.; Xi, B.; Song, Y.; Campana, C.; Zuo, J.-L.; Ren, T. *Angew. Chem., Int. Ed.* **2010**, *49*, 954.
(60) Olivier, C.; Costuas, K.; Choua, S.; Maurel, V.; Turek, P.; Saillard, J.-Y.; Touchard, D.; Rigaut, S. *J. Am. Chem. Soc.* **2010**, *132*, 5638. Olivier, C.; Choua, S.; Turek, P.; Touchard, D.; Rigaut, S. *Chem. Commun.* **2007**, 3100.
(61) Rigaut, S.; Olivier, C.; Costuas, K.; Choua, S.; Fadhel, O.; Massue, J.; Turek, P.; Saillard, J.-Y.; Dixneuf, P. H.; Touchard, D. *J. Am. Chem. Soc.* **2006**, *128*, 5859. Vacher, A.; Benameur, A.; M. Ndiaye, C.; Touchard, D.; Rigaut, S. *Organometallics* **2009**, *28*, 6096. Rigaut, S.; Massue, J.; Touchard, D.; Fillaut, J.-L.; Golhen, S.; Dixneuf, P. H. *Angew. Chem., Int. Ed.* **2002**, *41*, 4513.

(62) Field, L. D.; Magill, A. M.; Shearer, T. K.; Colbran, S. B.; Lee, S. T.; Dalgarno, S. J.; Bhadbhade, M. M. *Organometallics* **2010**, *29*, 957.
(63) Kim, B.-S.; Beebe, J. M.; Olivier, C.; Rigaut, S.; Touchard, D.; Kushmerick, J. G.; Zhu, X.-Y.; Frisbie, C. D. *J. Phys. Chem. C* **2007**, *111*, 7521.
(64) Liu, K.; Wang, X.; Wang, F. *ACS Nano* **2008**, *2*, 2315.
(65) Mahapatro, A. K.; Ying, J.; Ren, T.; Janes, D. B. *Nano Lett.* **2008**, *8*, 2131.
(66) Luo, L.; Benameur, A.; Brignou, P.; Choi, S. H.; Rigaut, S.; Frisbie, C. D. *J. Phys. Chem. C* **2011**, *115*, 19955.
(67) Olivier, C.; Kim, B.-S.; Touchard, D.; Rigaut, S. *Organometallics* **2008**, *27*, 509. Benameur, A.; Brignou, P.; Di Piazza, E.; Hervault, Y.-M.; Norel, L.; Rigaut, S. *New J. Chem.* **2011**, *35*, 2105.
(68) Gauthier, N.; Tchouar, N.; Justaud, F.; Argouarch, G.; Cifuentes, M. P.; Toupet, L.; Touchard, D.; Halet, J.-F.; Rigaut, S.; Humphrey, M. G.; Costuas, K.; Paul, F. *Organometallics* **2009**, *28*, 2253.
(69) Kobatake, S.; Uchida, K.; Tsuchida, E.; Irie, M. *Chem. Commun.* **2002**, 2804−2805.
(70) The amount of long-range charge transfer of the excited states in **1**, **2**, and **4**, which is due to the presence of the aryl-acetylide substituent on the Ru atoms, could not be correctly handled by TDDFT calculations.
(71) (a) Winter, R. F.; Klinkhammer, K. W. *Organometallics* **2001**, *20*, 1317. (b) Auger, N.; Touchard, D.; Rigaut, S.; Halet, J.-F.; Saillard, J.-Y. *Organometallics* **2003**, *22*, 1638.
(72) As a matter of fact, though sample solutions of the complex **5o** in CH_2Cl_2 were irradiated at 350, 540, 680, and 750 nm for 2 h, no change were observed.
(73) (a) Indelli, M. T.; Carli, S.; Ghirotti, M.; Chiorboli, C.; Ravaglia, M.; Garavelli, M.; Scandola, F. *J. Am. Chem. Soc.* **2008**, *130*, 7286−7299. (b) Motoyama, K.; Li, H.; Koike, T.; Hatakeyama, M.; Yokojima, S.; Nakamura, S.; Akita, M. *Dalton Trans.* **2011**, *40*, 10643.
(74) D'Amico, C.; Lorenc, M.; Collet, E.; Green, K. A.; Costuas, K.; Mongin, O.; Blanchard-Desce, M.; Paul, F. *J. Phys. Chem. C* **2012**, *116*, 3719.
(75) Richardson, D. E.; Taube, H. *Inorg. Chem.* **1981**, *20*, 1278.
(76) (a) Using the DigiElch simulation software (Elchsoft). (b) Rudolph, M. *J. Comput. Chem.* **2005**, *26*, 1193.
(77) From comparison with the monoelectronic reversible oxidation of decamethylferrocene.
(78) (a) Actually, for a molecule containing two strictly identical and noninteractiong redox sites, the two electrons cannot be transferred at the same potential, but the second electron is usually transferred at a more positive potential (for an oxidation) with a peak potential difference equal to (RT/F) ln 4 = 35.6 mV at 298 K (unless the second electronic transfer is more favorable for exactly this value). This value is due to an entropic factor, resulting from the fact that there are two possibilities for removing the first electron and only one left for the second one. (b) Ammar, F.; Savéant, J.-M. *J. Electroanal. Chem.* **1973**, *47*, 115.
(79) Rigaut, S.; Maury, O.; Touchard, D.; Dixneuf, P. H. *Chem. Commun.* **2001**, 373. Rigaut, S.; Perruchon, J.; Guesmi, S.; Fave, C.; Touchard, D.; Dixneuf, P. H. *Eur. J. Inorg. Chem.* **2005**, 447.
(80) The 4+ states were not investigated for solubility and stability reasons.
(81) Maurer, J.; Linseis, M.; Sarkar, B.; Schwederski, B.; Niemeyer, M.; Kaim, W.; Záliš, S.; Anson, C.; Zabel, M.; Winter, R. F. *J. Am. Chem. Soc.* **2008**, *130*, 259.
(82) Giraud, M.; Léaustic, A.; Guillot, R.; Yu, P.; Dorlet, P.; Métivier, R.; Nakatani, K. *New J. Chem.* **2009**, *33*, 1380.
(83) Savéant, J.-M. In *Elements of Molecular and Biomolecular Electrochemistry*; John Wiley and Sons: Hoboken, 2006.
(84) (a) In other words, over the range of scan rates studied, the chemical process following the heterogeneous electron transfer is not necessarily rate-limiting. It may be a competition between diffusion and follow-up reaction. (b) Andrieux, C. P.; Nadjo, L.; Savéant, J.-M. *J. Electroanal. Chem.* **1973**, *42*, 223. (c) Andrieux, C. P.; Savéant, J.-M. Electrochemical reactions. In *Investigations of Rates and Mechanism of Reactions*; Bernasconi, C. F., Ed.; Wiley: New York, 1986; Vol. *6*, 4E, Part 2.
(85) Ishibashi, Y.; Fujiwara, M.; Umesato, T.; Saito, H.; Kobatake, S.; Irie, M.; Miyasaka, H. *J. Phys. Chem. C* **2011**, *115*, 4265. Shim, S.; Eom, I.; Joo, T.; Kim, E.; Kim, K. S. *J. Phys. Chem. A* **2007**, *111*, 8910. Shim, S.; Joo, T.; Bae, S. C.; Kim, K. S.; Kim, E. *J. Phys. Chem. A* **2003**, *107*, 8106.
(86) Green, K. A.; Cifuentes, M. P.; Corkery, T. C.; Samoc, M.; Humphrey, M. G. *Angew. Chem., Int. Ed.* **2009**, *48*, 7867.
(87) Osuka, A.; Fujikane, D.; Shinmori, H.; Kobatake, S.; Irie, M. *J. Org. Chem.* **2001**, *66*, 3913.
(88) Wong, M. S.; Nicoud, J.-F. *Tetrahedron Lett.* **1994**, *35*, 6113.
(89) Higgins, S. J.; La Pensée, A.; Stuart, C. A.; Charnock, J. M. *Dalton Trans.* **2001**, 902.
(90) Touchard, D.; Haquette, P.; Guesmi, S.; Le Pichon, L.; Daridor, A.; Toupet, L.; Dixneuf, P. H. *Organometallics* **1997**, *16*, 3640.
(91) Garreau, D.; Savéant, J.-M. *J. Electroanal. Chem.* **1972**, *35*, 309.
(92) Connelly, N. G.; Geiger, W. E. *Chem. Rev.* **1996**, *96*, 877.
(93) (a) te Velde, G.; Bickelhaupt, F. M.; van Gisbergen, S. J. A.; Fonseca Guerra, C.; Baerends, E. J.; Snijders, J. G.; Ziegler, T. *J. Comput. Chem.* **2001**, *22*, 931. (b) Fonseca Guerra, C.; Snijders, J. G.; te Velde, G.; Baerends, E. J. *Theor. Chem. Acc.* **1998**, *99*, 391. (c) *ADF2013*; SCM, Theoretical Chemistry; Vrije Universiteit, Amsterdam, The Netherlands, http://www.scm.com.
(94) (a) Noodleman, L.; Davidson, E. *Chem. Phys.* **1986**, *109*, 131. (b) Ciofini, I.; Daul, C. *Coord. Chem. Rev.* **2003**, *238*, 187−209. (c) Neese, F. *Coord. Chem. Rev.* **2009**, *253*, 526−563. (d) Onofrio, N.; Mouesca, J.-M. *J. Phys. Chem. A* **2010**, *114*, 6149−6156. (e) Ruiz, E.; Cano, J.; Alvarez, S.; Alemany, P. *J. Am. Chem. Soc.* **1998**, *120*, 11122−11129. (f) Onofrio, N.; Mouesca, J.-M. *Inorg. Chem.* **2011**, *50*, 5577.
(95) Vosko, S. H.; Wilk, L.; Nusair, M. *Can. J. Phys.* **1980**, *58*, 1200.
(96) Becke, A. D. *Phys. Rev. A* **1988**, *38*, 3098. Perdew, J. P. *Phys. Rev. B* **1986**, *33*, 8822.
(97) Verluis, L.; Ziegler, T. *J. Chem. Phys.* **1988**, *88*, 322.
(98) van Lenthe, E.; Baerends, E. J. *J. Comput. Chem.* **2003**, *24*, 1142.
(99) van Gisbergen, S. J. A.; Snijders, J. G.; Baerends, E. J. *Comput. Phys. Commun.* **1999**, *118*, 119.
(100) Perdew, J. P.; Burke, K.; Ernzerhof, M. *Phys. Rev. Lett.* **1996**, *77*, 3865. Hammer, B.; Hansen, L. B.; Norskov, J. K. *Phys. Rev. Lett.* **1999**, *B59*, 7413.